To my family

DEVELOPMENT OF THERAPEUTIC STRATEGIES AGAINST CRIMEAN-CONGO HEMORRHAGIC FEVER (CCHF)

A THESIS SUBMITTED TO

THE GRADUATE SCHOOL OF ENGINEERING AND SCIENCE

OF BILKENT UNIVERSITY

IN PARTIAL FULFILLMENT OF THE REQUIREMENTS FOR

THE DEGREE OF

MASTER OF SCIENCE

IN

MATERIALS SCIENCE AND NANOTECHNOLOGY

By

ECE AVCI

AUGUST 2024

DEVELOPMENT OF THERAPEUTIC STRATEGIES AGAINST CRIMEAN-CONGO HEMORRHAGIC FEVER (CCHF)

By Ece Avcı

August 2024

We certify that we have read this dissertation and that in our opinion it is fully adequate, in scope and in quality, as a thesis for the degree of Master of Science.

_____
Urartu Özgür Şafak Şeker (Advisor)

_____
Serkan İsmail Göktuna

_____
Aykut Özkul

Approved for the Graduate School of Engineering and Science:

_____

Orhan Arıkan
Director of the Graduate School

ABSTRACT

DEVELOPMENT OF THERAPEUTIC STRATEGIES AGAINST CRIMEAN-CONGO HEMORRHAGIC FEVER (CCHF)

Ece Avcı

M.Sc in Materials Science and Nanotechnology

Advisor: Urartu Özgür Şafak Şeker

August, 2024

Crimean-Congo Hemorrhagic Fever (CCHF) is a highly fatal and zoonotic arboviral infection in humans. It is caused by the CCHF virus, which precipitates severe hemorrhagic outbreaks with a mortality rate reaching up to 40%. CCHF is classified as an arboviral disease due to its transmission through tick vectors of the *Hyalomma* species, which are arthropods. Human infection occurs either via bites from infected ticks or through exposure to the bodily fluids of infected animals or patients. Since the initial reported case in Turkey in 2002, a total of 9,700 cases have been documented. The disease is endemic in Turkey, positioning it as one of the most affected countries by CCHF within the European region. Currently, there is no effective protective measure, such as a vaccine or specific antiviral treatment, for CCHF. This lack of

effective countermeasures constitutes a significant public health threat and a serious sociological issue.

The aim of this study is to develop virus-specific and host-safe strategies against CCHF to directly inhibit virus infection and/or subsequent treatment of the disease. For this purpose, the CRISPR/Cas13b genome editing tool will be utilized. RNA editing systems, such as CRISPR-Cas13b, offer the advantage of controlling gene expression without altering the underlying DNA sequence and can exert transient modifications at the RNA level, making them promising tools in combating RNA viruses. The two virus genome segments, the S segment, which encodes the nucleocapsid protein to protect and organize the viral genome, and the L segment, which encodes RNA polymerase for replication and transcription processes necessary for viral propagation, will be rendered ineffective using the CRISPR/Cas tool. Finally, to demonstrate the inhibition of CCHFV replication in HEK293 cells via the CRISPR/Cas13b system, recombinant adeno-associated virus (rAAV) will be used as the gene delivery agent. If the proposed hypothesis is confirmed, the project will significantly impact the country with the know-how generated.

Keywords: Crimean-Congo Hemorrhagic Fever, Therapeutic Strategy, CRISPR/Cas, AAV-Mediated Gene Delivery

ÖZET

KIRIM-KONGO KANAMALI ATEŞİNE (KKKA) KARŞI TEDAVİ STRATEJİLERİNİN GELİŞTİRİLMESİ

Ece Avcı

Malzeme Bilimi ve Nanoteknoloji, Yüksek Lisans

Tez Danışmanı: Urartu Özgür Şafak Şeker

Ağustos, 2024

Kırım-Kongo Kanamalı Ateşi (KKKA), insanlarda oldukça ölümcül ve zoonotik bir arboviral enfeksiyondur. CCHF virüsünün neden olduğu bu hastalık, %40'a kadar ulaşan ölüm oranıyla şiddetli kanamalı salgınlara yol açmaktadır. KKKA, *Hyalomma* türüne ait keneler aracılığıyla bulaşması nedeniyle bir arboviral hastalık olarak sınıflandırılır. İnsan enfeksiyonu, enfekte kenelerin ısırması veya enfekte hayvanların ya da hastaların vücut sıvılarına maruz kalma yoluyla gerçekleşir. Türkiye'de ilk bildirilen vakadan bu yana 2002 yılında, toplamda 9.700 vaka kaydedilmiştir. Hastalık Türkiye'de endemik olup, ülkeyi Avrupa bölgesinde KKKA'dan en çok etkilenen ülkelerden biri konumuna getirmiştir. Şu anda KKKA'ya karşı etkili bir koruyucu önlem, aşı veya spesifik antiviral tedavi bulunmamaktadır. Bu etkili karşı önlemlerin yokluğu, önemli bir halk sağlığı tehdidi ve ciddi bir sosyolojik sorun teşkil etmektedir.

Bu çalışmanın amacı, CCHF'ye karşı virüs spesifik ve konakçıya güvenli stratejiler geliştirmek, virüs enfeksiyonunu doğrudan inhibe etmek ve/veya hastalığın sonrasındaki tedavisini gerçekleştirmektir. Bu amaç doğrultusunda, CRISPR/Cas13b genom düzenleme aracı kullanılacaktır. CRISPR-Cas13b gibi RNA düzenleme sistemleri, gen ekspresyonunu DNA dizilimini değiştirmeden kontrol etme avantajı sunar ve RNA düzeyinde geçici modifikasyonlar uygulayabilir, bu da onları RNA virüsleriyle mücadelede umut verici araçlar haline getirir. Virüs genom segmentlerinden S segmenti, viral genomu korumak ve organize etmek için nükleokapsid proteinini kodlar, ve L segmenti ise, viral çoğalma ve transkripsiyon süreçleri için gerekli olan RNA polimerazı kodlar. Bu iki segment CRISPR/Cas aracı ile etkisiz hale getirilecektir. Son olarak, CRISPR/Cas13b sistemi aracılığıyla HEK293 hücrelerinde CCHFV replikasyonunun inhibisyonunu göstermek için, gen aktarım ajanı olarak rekombinant adeno-ilişkili virüs (rAAV) kullanılacaktır. Önerilen hipotez doğrulanırsa, proje ülkede önemli bir etki yaratacak ve elde edilen bilgi birikimi ile anlamlı bir katkı sağlayacaktır.

Anahtar Kelimeler: Kırım-Kongo Kanamalı Ateşi, Tedavi Stratejisi, CRISPR/Cas, AAV-Aracılı Gen Transfer

ACKNOWLEDGEMENTS

First and foremost, I am profoundly grateful to Asst. Prof. Urartu Özgür Şafak Şeker. I vividly remember attending his synthetic biology courses, where his passion ignited my curiosity. I approached him with the hope of joining his research group. His acceptance was a pivotal moment in my academic journey. Under his guidance, I found myself in an environment that was not only conducive to research but also nurturing of young scientists' ideas. His wisdom, patience, and vision have profoundly influenced my development as a scientist. I am deeply thankful for his invaluable support and for helping shape my career trajectory.

I would also like to extend my heartfelt thanks to the members of my thesis jury, Prof. Aykut Özkul, and Asst. Prof. Serkan Göktuna. Their insightful feedback, constructive criticism, and thoughtful questions during my defense have been invaluable. I am deeply grateful for the time and effort they dedicated to reviewing my work and their contributions to my academic growth. I would also like to thank Prof. Aykut Özkul and Dr. Sıdıka Öztop, our collaborators in this project. Their expertise and support were instrumental in the successful completion of my thesis.

To the current members of the Synthetic Biosystems Laboratory, working with such a friendly and inspiring group of people has been an incredible experience. I especially want to thank Gizem Makas for her kindness, assistance, and support. I would like to give special thanks to some members of the SBL. İlkay Çisil Köksaldı, for her incredible effort and support, when I was a newbie to the lab. She took me under her wing, teaching me everything and becoming a dear friend. Visiting her during my vacation to Basel was a wonderful experience as we reminisced about the times when I was her Padawan. Ahmet Hınçer, for his unwavering assistance with every silly question I had and significant help throughout this project. Ahmet is one of the most intelligent people I have ever met, and I am truly fortunate to call him a friend. Derin Akman, my lab bestie, for our fantastic coffee breaks and shared rakı dates. Your friendship and these moments of relaxation and joy have made my time in the lab truly special. Nazlıcan and Damla, for being the best roommates and for forgiving me for almost burning down the house while cooking!

My heartfelt thanks go to my mother, Yeşim Avcı. She is the strongest woman I have ever known. I can't count the number of times I have called her on the phone to ask for advice on everything. Whenever something goes wrong in life, she always tells me it's going to be okay, and just hearing that from her makes everything better. Our bond is so deep that she is not only my mother but also my best friend. As a scientist, I have a very strict and materialistic view of life, while she embraces a deeply spiritual perspective which provides me with a new way to look at things. Her wisdom, patience, and unconditional love have been my guiding light. I am incredibly lucky to be her

daughter, I look up to her in every way and hope that one day I can be as wonderful a mother as she is. To my sister, Küçük Ezgi, from the day she was born, she brought immense joy to our family. I immediately felt the responsibility of being a big sister. There is nothing I wouldn't do for her. Growing up with her was a blessing, and we were inseparable during our childhood. Now, having lived away from her for the past seven years, it feels so strange and often difficult. Even though she is just three years younger than me, it feels like there are many more years between us, and I still see her as my baby sister. But I know she is not a baby anymore. She has grown into a wonderful person, ready to take on the world. Though writing these words makes me emotional, they are filled with love and hope for her future. Our bond is unbreakable, and no matter the distance, she will always be a part of me.

To my boyfriend, Ege. I feel so incredibly lucky to have met such a loving and selfless person. His signature cocktails, delicious scrambled eggs, and the cutest good morning texts have become delightful parts of my life, adding a special touch to our time together. We connected on a deeper level, and I am grateful for his unwavering support during the stressful times of writing this thesis. I cannot thank him enough for being by my side.

In conclusion, I have had many thanks to give. This thesis is not just a culmination of my academic efforts but a reflection of the collective support, love, and guidance I have received from many remarkable people. I would like to finish with a science quote I love: "The good thing about science is that it's true whether you believe it or not."

Table of Contents

Contents

LIST OF TABLES

LIST OF FIGURES

CHAPTER I: INTRODUCTION

1.1 Crimean Crimean-Congo Hemorrhagic Fever (CCHF)

Crimean-Congo Hemorrhagic Fever (CCHF) is a fatal arboviral infectious disease of global health concern. CCHF is classified as an arboviral disease since it is transmitted through a tick vector of *Hyalomma* species, which is an arthropod [1]. One study suggests that the fatality rate of the disease is >40%; however, the rate may vary according to factors such as the strain of the virus, location, and access to healthcare [2].

The first clinical description of the disease dates back to 1944 when a devastating outbreak of over 200 cases was reported in the West Crimea region of the former Soviet Union among farmers [3]. In 1956, a viral isolate from a teenage boy was studied and named V3011 in Belgian Congo by Dr. Courtois [4]. Characterization studies on mice carried out at Yale University shed light on the antigenic similarity between the viral isolates. The two regions where the virus was isolated later led to the adoption of the name "Crimean-Congo" [5].

The disease can be characterized by the following clinical symptoms that progress rapidly: An onset of high fever accompanied by a severe headache will be experienced by patients, followed by significant bleeding from the skin, nasopharynx, nose, mouth, and gastrointestinal tract, termed infamously as "hemorrhage" [6,7]. As the disease progresses, a hemorrhagic rash may develop, as well as ecchymoses, meaning skin discoloration from damaged, leaking blood vessels underneath the skin. Individuals

may experience fatigue and myalgia (muscle pain). Gastrointestinal symptoms may lead to nausea and vomiting. A decrease in the number of blood cells such as platelets (thrombocytopenia) and white blood cells (leukopenia) is also a common symptom. Lastly, liver involvement indicated by elevated enzymes such as alanine transaminase (ALT) and aspartate aminotransferase is observed.

Although the timeline of the disease symptoms may vary from patient to patient, an outline of the course of the disease can be described in four major phases: the incubation phase, pre-hemorrhagic phase, hemorrhagic phase, and recovery phase [6]. Exposure to CCHFV will lead to an incubation phase that may last from 3 days to a week, during which the symptoms explained above will not be experienced [8]. The pre-hemorrhagic phase is when initial nondescript symptoms such as headache, chills, myalgia, and fever emerge following the incubation period. In the hemorrhagic phase, symptoms such as nausea, vomiting, fatigue, and varying degrees of hemorrhage will be observed. Organs such as the liver may get involved, leading to disseminated intravascular coagulation and possibly organ failure. About 20 days post-illness, the recovery phase begins with ongoing fatigue, nausea, loss of hearing, memory, appetite, and disrupted vision [9].

Since it was first reported in 2002, CCHF has been of great interest as it is endemic to Turkey with a fatality rate of 5% [10,11]. An endemic disease is consistently present in a particular area. Although the patterns of occurrence may change over time, an endemic disease will show a stable presence within the population due to specific risk factors or environmental conditions that support its continued presence. Turkey has established a foundation for the circulation of the disease, leading to sporadic outbreaks since the emergence of the disease [12]. Numerous factors influence the endemicity of CCHF in Turkey. Turkey's geographical location is suitable for the thriving of suitable

tick vectors and animal reservoirs, which aid in the survival and transmission of the CCHFV [13]. CCHF also appears to rise as a problem seasonally in certain regions of the country due to high tick activity as well as human exposure at specific times of the year [14]. As farming is an important sector in Turkey, the risk of zoonotic transmission of the disease is increased by the close interaction between livestock, tick vectors, and humans. Another factor contributing to the endemic nature of CCHF is the public health challenge of controlling tick populations and human-animal interactions. Understanding the above-mentioned factors is crucial for taking preventive measures while combating CCHF.

The causative agent of CCHF is the Crimean-Congo Hemorrhagic Fever Virus (CCHFV), which is classified within the order *Bunyavirales*, family *Nairoviridae*, and genus *Orthonairovirus*. The virus is characterized by its single-stranded, negative-sense, three-part RNA genome. The genome of negative-sense RNA viruses is complementary to the viral mRNA and cannot be translated directly by the host's translation machinery [15]. The virion has a spherical shape of around 100 nm in diameter depicted in Figure 1 [16]. The nucleoprotein (NP) encapsulates the three single-stranded RNA segments: small (S), medium (M), and large (L). The S segment (1.7 kb) encodes the NP, which aids RNA binding through the globular domain, assembly of the viral nucleic acid, as well as viral replication and mRNA transcription [17–19]. It is also the primary viral antigen to elicit humoral immunity during infection, making it a target for diagnostic studies. The size of the M segment is around 5.3 kb [19]. It encodes the glycoproteins GN and GC that help bind cellular receptors of the host [6]. During infection, neutralizing antibodies are produced against these glycoproteins, which are embedded in the lipid envelope. The 12 kb large (L) segment codes for the RNA-dependent RNA polymerase (RdRp) that is responsible for

producing new viral RNA strands during replication, propagating the virus inside host cells [19,20].

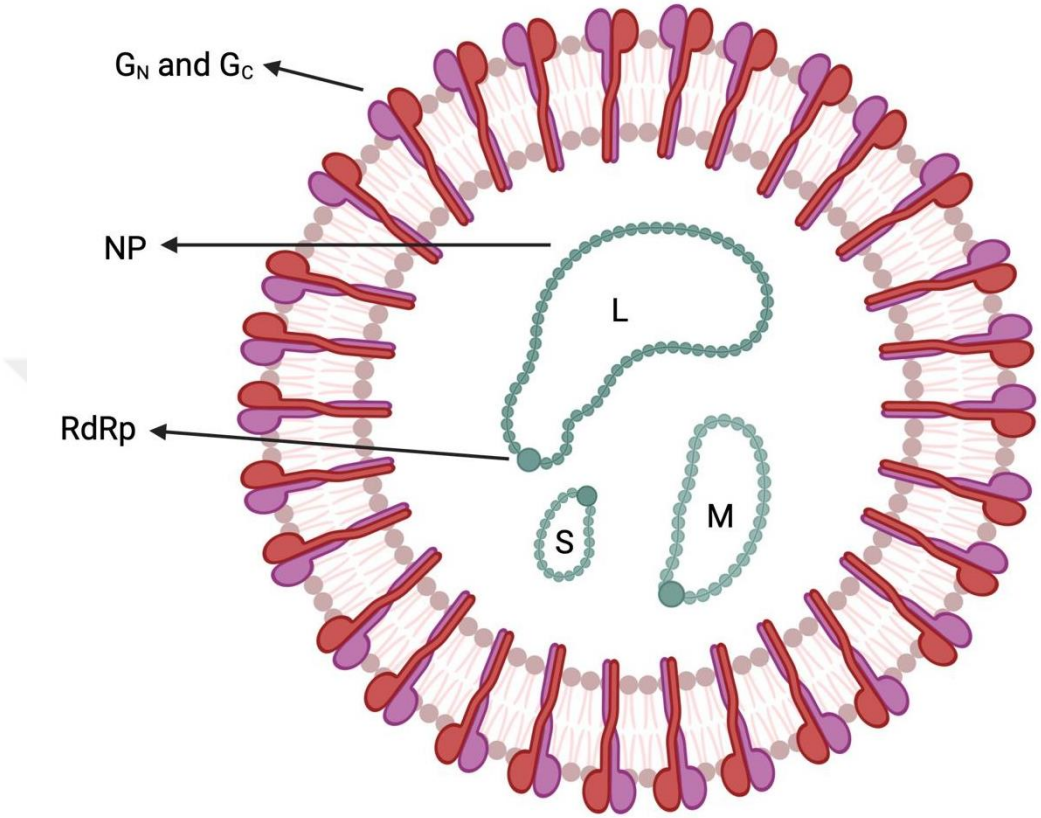

Figure 1: A closer look inside a CCHF virion, with a diameter of 80-100 nm, reveals its tripartite genome: S, M, and L segments. The glycoproteins (G_N and G_C) play vital roles in the viral life cycle, such as attachment to the host cell, entry into the host cell, and immune evasion. The nucleoprotein (NP) is responsible for the protection and packaging of viral RNA, while the RNA-dependent RNA polymerase (RdRp) assists in the replication of the viral genome. Illustration is created using BioRender.com.

Replication starts with the binding of viral particles to host cell surface receptors through glycoproteins, followed by clathrin-dependent endocytosis [21,22]. Inside the endosome, the low pH helps the fusion between the virion and endosome and eventually the release of nucleocapsids to the cytoplasm. Here, RdRp starts synthesizing the complementary positive strands that serve as mRNA intermediates and are later used as templates for the negative-sense strand synthesis. The mRNA is then used for the translation of viral proteins, and cRNA (complementary RNA) serves as a template for viral genome formation [23,24]. As new nucleotide sequences are synthesized, the capsid proteins encapsidate the vRNA (viral RNA).

The host of the Crimean-Congo Hemorrhagic Fever Virus is *Hyalomma* spp. ticks. Humans may get infected with the virus either by tick bites of an infected tick or by exposure to body fluids of infected animals or patients [6]. People in rural areas, especially farmers, animal herders, livestock, and slaughterhouse workers, are at risk. Some prevention strategies recommended by the Republic of Turkey Ministry of Health include wearing clothes that cover the entire body when entering areas of high risk, such as gardens, forests, and vineyards [25]. Wearing light-colored clothes also helps to easily spot ticks. Check yourself for any ticks sticking behind your ears and knees. In case of finding a tick, medical help should be sought immediately. Ticks should be removed by fine-tipped tweezers without crushing. Contact with animals' blood, body fluids, and tissues should be avoided to decrease the risk of transmission.

Clinicians take a multifaceted approach to laboratory testing and clinical evaluation for the diagnosis of CCHF. The two laboratory testing methods utilized are the quantitative reverse transcription polymerase chain reaction (qRT-PCR) for the detection of viral RNA in patient samples and enzyme-linked immunosorbent assay (ELISA) performed

against CCHFV antibodies such as IgG and IgM that are available during the first 10 days of the disease when patients are viremic (the virus is present in the blood) [6,26,27]. Clinical evaluation of characteristic symptoms such as severe fever, hemorrhage, and increased levels of ALT and AST also aid in diagnosis [6,7]

Currently, there is a lack of specific antiviral treatment options for CCHF. The drug named ribavirin, which was initially designed for the treatment of respiratory syncytial virus and hepatitis C, shows promise and is recommended for early treatment of high-risk cases, especially for post-exposure prophylaxis as well as hematemesis (vomiting blood) [10].

1.2 CRISPR/Cas Genome Editing Tool

Ever since it was discovered, CRISPR (Clustered Regularly Interspaced Short Palindromic Repeats) has been utilized as a precise genome editing tool and revolutionized genetic research. In 1987, Ishino and his colleagues came across strange repeat sequences interspaced by spacer sequences while studying alkaline phosphatase in *E. coli* [28]. The role of this unique array in bacterial immunity against invading bacteriophages remained a mystery until the early 2000s. In 1993, it was discovered that these sequences were conserved in another domain of life, archaea [29] The origin of the CRISPR sequences was described as deriving from pre-existing foreign genetic elements [30]. Continuing work focused on identifying four genes that are CRISPR-associated (Cas). These genes were shown to be functionally related to CRISPR loci as they are located nearby [31] .Later in the genomic era, it was shown that CRISPR, together with Cas proteins, comprises an acquired defense mechanism where foreign gene elements integrate into the host genome to provide immunity against respective

agents during the course of evolution [32]. Notably, in organisms that encode Cas proteins, genes could be silenced using CRISPR-Cas systems.

Currently, there are two main classes and six types of CRISPR-Cas systems. The classifications are based on the type of effector complex each system has. Class one systems (Types I, III, IV) work with multiple subunit effectors, while Class two systems (Type 5- Cas12, Type VI-Cas13b, Type II-Cas9) rely on single-component effectors [33].

In 2020, Emmanuelle Charpentier and Jennifer Doudna won the Nobel Prize in Chemistry for their work on CRISPR-Cas9 gene-editing technology. Their technique based on CRISPR-Cas9 was referred to as "molecular scissors" as it laid the foundation for precise and efficient editing of DNA using the Cas9 enzyme [34]. After this study, genomic manipulations were no longer a bottleneck to experiments, and a new era for human therapeutics and biotechnology began.

In 2017, the CRISPR-Cas13b two-component ribonuclease system was introduced: the RNA-guided RNA-targeting Cas13b family of effector proteins and their single crRNA (CRISPR RNA) that helps target and cleave specific RNA sequences [35]. Single-stranded RNA cleavage by Cas13b nuclease is triggered upon recognition of a 24-30 nucleotide sequence on the target RNA sequence [35,36]. Cas13b proteins are classified into several types: Cas13ba, Cas13b, Cas13bc, Cas13bd, Cas13bx, and Cas13by [37]. The Cas13b protein has 1150 amino acids and prefers a double PFS (Protospacer Flanking Site) that is an A, U, or G in 5’ and NAN or NNA in 3’ [38]. RNA degradation activity is provided by HEPN (Higher Eukaryotes and Prokaryotes Nucleotide-binding) domains. If HEPN domains are mutated, the Cas13b protein will be rendered

catalytically inactive but will still be able to bind RNA sequences, which is useful in RNA-based detection, RNA imaging, and modification studies [39].

Currently, the detection of viral infections is highly problematic as molecular tests are not broadly available. CRISPR has come to the stage to find rapid and low-cost detection solutions as conventional methods such as ELISA and RT-qPCR require professional laboratory personnel and are highly time-consuming [38]. The SHERLOCK (Specific High-Sensitivity Enzymatic Reporter UnLOCKing) method was developed as a CRISPR-Cas13b system-based nucleic acid detection system [40]. To serve as a point-of-care pathogen detection system, the Cas13ba enzyme detected strains of Zika and Dengue viruses as well as bacterial pathogens from serum or urine samples. The described system relied on Cas13ba-mediated collateral cleavage and sensitive nucleic acid RPA (Recombinase Polymerase Amplification) to detect reporter RNA molecules. This platform is promising for further applications such as the detection of infectious diseases and genotyping.

On the contrary, Cas13b is shown not to lead to collateral damage. It shows reduced collateral RNA cleavage in mammalian cells compared to other Cas13b enzymes. Research on variants like PspCas13b highlights their high specificity and minimal off-target effects in HEK293 cells [41]. Structural differences and regulatory mechanisms make Cas13b precise for RNA interference, minimizing collateral damage and making it a valuable tool for RNA-targeting in mammalian systems.

Later in 2020, the CARMEN (Combinatorial Arrayed Reactions for Multiplexed Evaluation of Nucleic Acids) platform was developed for multiplexed detection of pathogens [42]. This Cas13b-based multiplex detection platform was able to detect all 169 human-associated viruses. The comprehensive study worked on samples amplified

with PCR or RPA mixed with Cas13b enzyme and corresponding crRNAs. The mixed samples were then added to colored solutions and loaded onto a microwell-array chip to be monitored with fluorescence microscopy.

The REPAIR (RNA Editing for Programmable A to I Replacement) platform was introduced as an RNA-editing platform that relies on a catalytically inactive Cas13b (dCas13b) that enforces adenosine-to-inosine deaminase activity by ADAR2 (Adenosine Deaminase Acting on RNA type 2) in mammalian cells for editing transcripts bearing mutations [43]. This platform showed how genetic diseases can be treated at the RNA level by editing sequences and rescuing functional proteins.

RNA editing systems such as CRISPR-Cas13b have the advantage of controlling gene expression without changing the underlying DNA sequence, which means transient modifications at the RNA level [35]. Compared to traditional RNAi technologies, CRISPR-Cas13b was shown to have greater RNA knockdown efficiency [44]. Therefore, CRISPR-Cas13b is the most promising tool in the toolbox of scientists trying to combat RNA viruses.

The CRISPR-Cas13b system has not only been used for diagnostic purposes but also for antiviral studies to combat several viruses [38]. Combating viral diseases has always been a hurdle as the viruses evolve quickly and render vaccines ineffectual. Viral drugs are the only clinical weapon humans have against viral infections now. However, resistance may develop against these drugs, and antiviral drug design requires an exhaustive understanding and mapping of virus infections [38]. A promising 2018 study showed that the Cas13ba nuclease can be programmed to target two viral pathogens: influenza virus A and human respiratory syncytial virus [45]. Guided by respective crRNAs, Cas13ba successfully alleviated viral infections during the course of

prophylaxis. The study also underlined the issue of inaccessibility of viral RNA in cells, which calls for careful screening of crRNAs to find those with compatible secondary structures as well as sequences. Following this study, efforts led to more CRISPR-Cas13b-based diagnostic studies against RNA viruses.

Below is a table describing all the work done using the CRISPR-Cas13b system along with their stated knockdown efficiency. As we can see, the Cas13b system offers great potential to be programmed and used against other RNA viruses, presenting a promising platform for combating viral infections that pose a threat to humans [46,47].

Table 1: Examples of Cas13b-based knockdown studies in several application fields

Cas13b Subtype	Organism	Description	Application
Cas13ba	*Leptotrichia wadei*	LwaCas13ba was shown to be the most efficient among other Cas13ba orthologs [48]	Knockdown in human cells
Cas13ba	*Leptotrichia wadei*	Knockdown of a nuclear lncRNA GACAT3 to determine its oncogenic properties [49]	Knockdown in human cells
Cas13ba	*Leptotrichia wadei*	Cas13ba NF-kB-driven expression. Knockdown of oncogenic *TERT*, *EZH2*, and *RELA* mRNAs [36]	Knockdown in human cells
Cas13ba	*Leptotrichia shahii*	Knockdown of CTG repeat-containing toxic mRNA [50]	Knockdown in human cells

Cas13b	*Prevotella* sp.	PspCas13b found to be most efficient among 43 variants of Cas13ba/b/c [43]	Knockdown in human cells
Cas13bd	*Ruminococcus flavefaciens*	Knockdown of endogenous transcripts in mouse embryos [51]	Knockdown in mouse cells
Cas13bd	*Ruminococcus flavefaciens*	Knockdown of metabolic genes *Pten*, *Pcsk9*, and liver enriched lncRNA *lncLstr* in mouse hepatocytes [52]	Knockdown of viruses
Cas13ba	*Leptotrichia buccalis*	Effective to reduce IAV and SARS-CoV-2 infection in mice and hamsters [53]	Knockdown of viruses
Cas13ba	*Leptotrichia shahii*	Effective with HIV [54]	Knockdown of viruses
Cas13ba	*Leptotrichia shahii*	Effective with HCV [55]	Knockdown of viruses
Cas13ba	*Leptotrichia wadei*	Effective knockdown of plant RNA virus TuMV in *Arabidopsis thaliana* and *Nicotiana benthamiana* [56]	Knockdown of viruses
Cas13ba	*Leptotrichia wadei*	Effective in downregulation of E6/E7 gene expression in HPV positive cell line [57]	Knockdown of viruses
Cas13ba	*Leptotrichia wadei*	Effective against DENV [58]	Knockdown of viruses
Cas13bd	*Ruminococcus flavefaciens*	Knockdown of SARS-CoV-2 and IAV in lung epithelial cells [59]	Knockdown of viruses

1.3 The Aim of Study

In this study, we aimed to develop novel therapeutic strategies against Crimean-Congo Hemorrhagic Fever (CCHF) by utilizing the CRISPR/Cas13b system to target and degrade viral RNA. Specifically, we focused on designing guide RNAs (gRNAs) to target the S segment of the CCHF virus genome, which encodes the nucleocapsid protein crucial for viral replication. Additionally, we aimed to optimize the delivery of CRISPR/Cas13b components to mammalian cells using adeno-associated virus (AAV) vectors due to their high transduction efficiency and safety profile. By incorporating Cas13b, gRNA, and direct repeat regions into an AAV expression vector and co-transfecting HEK293 cells, we sought to achieve efficient and sustained gene expression of CRISPR/Cas13b agents. Furthermore, we aimed to demonstrate the successful *in vitro* cleavage of viral RNA by the guided Cas13b activity, which is depicted in the detailed schematic in Figure 2. This comprehensive approach provides a foundation for future therapeutic applications against CCHF and other RNA viruses, ultimately contributing to the development of specific and safe antiviral strategies and enhancing our ability to combat viral infections more effectively.

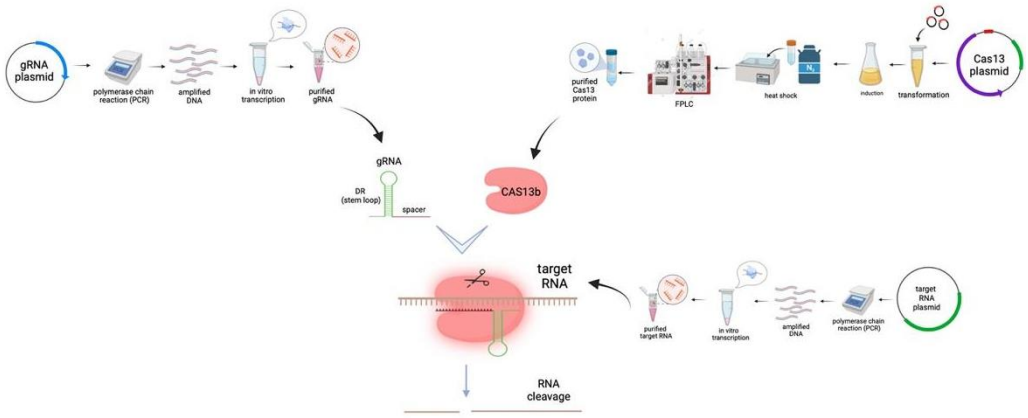

Figure 2: Schematic representation of the aim of the study: *in vitro* cleavage of RNA by guided Cas13b nuclease activity. The reaction contains three components: Cas13b expressed in *E. coli*, target RNA, and gRNA produced by IVT. Illustration created using BioRender.com

CHAPTER II: MATERIALS AND METHODS

2.1 Cell Strains, Growth, Transformation, and Cell Maintenance

Due to its high insert stability and high DNA yield, the *E. coli* DH5α strain was utilized throughout the cloning experiments. This strain contains the PRO cassette, encoding genes for the constitutive expression of TetR and LacI repressors, as well as the spectinomycin resistance gene. The *E. coli* BL21 DE3 strain was used for recombinant protein expression. The T7 polymerase gene under the control of the Lac promoter, encoded by this strain, along with the deficiency of Lon and OmpT proteases, makes it an excellent candidate for protein expression. All cell stocks were maintained in 25% glycerol in Lysogeny Broth (LB) solution (recipe given in Appendix E, Table E.1) at -80°C.

Plasmids were transformed into the aforementioned bacterial cells through chemical transformation. Chemically competent *E. coli* DH5α and *E. coli* BL21 DE3 cells were prepared by inoculating cells from -80°C stocks for overnight growth in LB medium supplied with respective antibiotics. The cells were then diluted 1:100 to grow in LB medium with antibiotics until the OD600 reached 0.2 - 0.5 and were chilled on ice for 10 minutes. Then, cells were centrifuged at 1000 x g for 10 minutes at 4°C and the supernatant was removed. The remaining cell pellet was resuspended in Transformation and Storage (TSS) Buffer (recipe given in Appendix E, Table E.5) with a 1:10 dilution. 100 µL aliquots of chemically competent cell solution were stored at -80°C for later transformations.

Upon thawing the chemically competent cells on ice, 100 ng of the desired plasmid was added, and the mixture was incubated on ice for 20 minutes. Cells were then subjected to a heat shock at 42°C for 45 seconds and immediately incubated on ice for 5 minutes to allow plasmid entry through opened pores. After adding 250 µL of LB, cells were incubated in a shaking incubator at 37°C and 200 rpm for 45 minutes. Cells were centrifuged at 8000 rpm for 5 minutes. All of the supernatant portion except for 100 µL was discarded, and the remaining cell pellet was resuspended in the 100 µL supernatant. Cells were spread onto LB-Agar plates (recipe given in Appendix E, Table E.1) containing respective antibiotics for overnight incubation at 37°C.

2.2 Construction of pET-22b(+)-RanCas13b-6His Vector

To construct the pET-22b(+)-RanCas13b-6His vector, the Addgene plasmid #103855 was purchased. RanCas13b was amplified using the specific primer pair with Q5 polymerase under recommended conditions (conditions provided in Appendix E, Table E7). 1000 ng of pET-22b(+)-GRFT-6His (plasmid available in our laboratory) was digested with XhoI (NEB) and KpnI-HF (NEB) restriction enzymes at 37°C for 2 hours (digestion reaction protocol given in Appendix E, Table E3). Digested DNA fragments and the PCR product were loaded in a 1% agarose gel containing SYBR™ Safe DNA gel stain for electrophoresis at 130V for 30 minutes. The expected bands on the agarose gel were cut out for DNA extraction using the Nucleospin Gel and PCR Clean-up kit (Macherey-Nagel), following the manufacturer's instructions. After measuring the concentration with the Thermo Scientific NanoDrop™ 2000 Spectrophotometer, the resulting linear DNA fragments were assembled via in-house Gibson Assembly (reaction mix protocol given in Appendix E, Table E4) at a 1:1 molar ratio. The Gibson assembly reaction was conducted at 50°C for 1 hour. Following the Gibson assembly

reaction, the mixture was transformed into chemically competent *E. coli* DH5α cells. Transformation steps are mentioned earlier, the cell stocks were prepared and stored at -80°C.

2.3 Construction of pET-22b(+)-gRNA-S Vector

The pET-22b(+)-gRNA-S construct was based on the existing pET-22b(+)-T7 plasmid. The RanCas13b Direct Repeat (DR) and gRNA sequences were cloned into the pET-22b(+)-T7 backbone by PCR with Q5 polymerase. The PCR product was loaded in a 1% agarose gel containing SYBR™ Safe DNA gel stain for electrophoresis at 130V for 30 minutes. The expected band on the agarose gel was cut out for DNA extraction using the Nucleospin Gel and PCR Clean-up kit (Macherey-Nagel), following the manufacturer's instructions. After measuring the concentration with the Thermo Scientific NanoDrop™ 2000 Spectrophotometer, the resulting linear DNA fragment was subjected to Gibson assembly at 50°C for 1 hour for circularization. The plasmid map is provided in Figure C.2. Following the Gibson assembly, the mixture was transformed into chemically competent *E. coli* DH5α cells. Transformation steps are mentioned earlier. Colonies were picked from the overnight incubated LB-Agar plate for Sanger sequence verification (Genewiz, USA). Verification data for colonies containing the RanCas13b gene were analyzed using Geneious Prime® (2021.1.1) software. Verified colonies were inoculated in 10 mL of LB medium containing appropriate antibiotics and incubated in a shaking incubator at 37°C and 200 rpm overnight. The next day, cell stocks were prepared and stored at -80°C.

2.4 Construction of pAAV-Cas13b-gRNA-L Vector

The pAAV-Cas13b-gRNA-L construct was cloned in two steps: first, Cas13b was cloned into the pAAV-MCS vector, followed by the cloning of the gRNA-expressing cassette into the resulting pAAV-Cas13b backbone. Cas13b was amplified from the pET-22b(+)-RanCas13b-6His backbone by PCR using Q5 polymerase. The PCR product was loaded onto a 1% agarose gel containing SYBR™ Safe DNA gel stain for electrophoresis at 130V for 30 minutes. The expected band on the agarose gel was cut out for DNA extraction using the Nucleospin Gel and PCR Clean-up kit (Macherey-Nagel), following the manufacturer's instructions. Three digestion reactions were then set up: Cas13b PCR product was double-digested with EcoRI-HF (NEB) and HindIII (NEB), the pAAV backbone was digested with MluI-HF (NEB) and EcoRI-HF (NEB), and the pAAV backbone was also digested with MluI-HF (NEB) and HindIII (NEB) restriction enzymes at 37°C for 2 hours (digestion reaction protocol given in Appendix E, Table E3). Digested DNA fragments of the pAAV backbone and the Cas13b PCR product were loaded onto a 1% agarose gel containing SYBR™ Safe DNA gel stain for electrophoresis at 130V for 30 minutes. The expected bands on the agarose gel were cut out for DNA extraction using the Nucleospin Gel and PCR Clean-up kit (Macherey-Nagel), following the manufacturer's instructions. After measuring the concentration with the Thermo Scientific NanoDrop™ 2000 Spectrophotometer, the resulting linear DNA fragments were ligated using a ligase enzyme (ligation protocol given in Appendix E, Table E8). Following the ligation reaction, the mixture was transformed into chemically competent *E. coli* DH5α cells. Transformation steps are mentioned earlier. Colonies were picked from the overnight incubated LB-Agar plate for Next Generation Sequencing (NGS). Verification data for colonies containing the RanCas13b gene were analyzed using Geneious Prime® (2021.1.1) software. Verified

colonies were inoculated in 10 mL of LB medium containing appropriate antibiotics and incubated in a shaking incubator at 37°C and 200 rpm overnight. The next day, cell stocks were prepared and stored at -80°C.

Next, the gRNA construct was generated using Addgene #78741 plasmid containing the U6 promoter. gRNA and DR regions were cloned into this vector by PCR using Q5 polymerase in two consecutive PCR reactions. The final PCR product was loaded onto a 2% agarose gel containing SYBR™ Safe DNA gel stain for electrophoresis at 130V for 30 minutes. The expected band on the agarose gel was cut out for DNA extraction using the Nucleospin Gel and PCR Clean-up kit (Macherey-Nagel), following the manufacturer's instructions. After measuring the concentration with the Thermo Scientific NanoDrop™ 2000 Spectrophotometer, the resulting gRNA construct and MluI-HF digested linear pAAV-Cas13b backbone were subjected to Gibson assembly at a 5:1 backbone

ratio at 50°C for 1 hour. Following the Gibson assembly, the mixture was transformed into chemically competent *E. coli* DH5α cells. Transformation steps are mentioned earlier. Colonies were picked from the overnight incubated LB-Agar plate for Sanger sequence verification (Genewiz, USA). Verification data for colonies containing the gRNA-DR genes were analyzed using Geneious Prime® (2021.1.1) software. The plasmid map is provided in Figure C.2. Verified colonies were inoculated in 10 mL of LB medium containing appropriate antibiotics and incubated in a shaking incubator at 37°C and 200 rpm overnight. The next day, cell stocks were prepared and stored at -80°C.

2.5 Sanger Sequencing, Next-Generation Sequencing (NGS) and Sequence Alignments

Once the cloning of a construct was completed, the inoculated colonies were used for plasmid isolation with the Thermo Scientific GeneJet Plasmid Miniprep Kit, following the manufacturer's instructions. The concentration of the isolated plasmid was measured using the Thermo Scientific NanoDrop™ 2000 Spectrophotometer. Based on the measured concentration, 1000 ng of plasmid was prepared for sequencing by mixing it with 5 µL of 5 µM sequencing primer and adjusting the final volume to 15 µL with dH2O. The samples were then sent to Genewiz (USA) for Sanger sequencing. The vector sequences were created and obtained from Benchling.com. The sequence files were acquired from the Genewiz company, and the .gb files exported from Benchling.com were imported using the file>import>from file option. This action opens a new window to navigate the files. The folder containing .abi files was selected to import all files. To align the two specific sequences, they were selected in the main working window. After selection, choosing to align/assemble>pairwise alignment from the upper panel opens a new window. In this window, users can define specific parameters to align the sequences. We opted for automatic direction determination, global alignments with free gaps, and 65% similarity to align the sequences.

To facilitate next-generation sequencing (NGS), the plasmids obtained through miniprep were submitted to the Intergen company in Ankara. A final volume of 20 µl, containing 1000-2000 ng of DNA, was dispensed into PCR tubes. The Geneious application was used to perform map-to-reference alignments, revealing significant pairwise identity scores exceeding 50% for key regions on the map. The consensus

sequence from this alignment was then uploaded to Benchling to enhance clarity regarding any mutations present.

2.6 Expression Optimization, Purification, and Quantitation of Cas13b Protein

Verified pET-22b(+)-RanCas13b-6His plasmid was transformed in both *E.coli* Rosetta and *E. coli* BL21 (DE3) cells to express the RanCas13b protein. Because RanCas13b was inserted downstream of the T7 promoter, protein expression was induced using Isopropyl-β-d-1-thiogalactopyranoside (IPTG), which activates the T7 promoter due to the T7 RNA polymerase gene being regulated by the Lac promoter. Cell stocks from -80°C of transformed Rosetta and BL21 (DE3) cells were inoculated into 5 ml LB medium containing 100 µg/ml ampicillin and incubated overnight at 37°C with continuous shaking at 200 rpm. The next day, 500 µl of the overnight culture of each cell was transferred into 50 ml LB medium with 50 µl ampicillin and incubated at 37°C for 4 hours, at 30°C for 8 hours, and at 18°C for 16 hours until the culture reached the mid-log phase (OD600: 0.4-0.6). Protein expression was then induced by adding IPTG to a final concentration of 1 mM (50 µl). Post-incubation, the cells were centrifuged at 8000 rpm for 5 minutes, and the pellet was resuspended in binding buffer (20 mM sodium phosphate, 0.5 M NaCl, 20 mM imidazole, pH 7.4). Phenylmethylsulfonyl fluoride (PMSF) (1 mM) and lysozyme (100 µg/µL) were added to the suspension. Cells were lysed through five freeze-thaw cycles using liquid nitrogen. The cell lysate was incubated on ice for 5 minutes and subjected to sonication at 30% amplitude with 10 seconds pulse on and 10 seconds pulse off for 5 minutes at 4°C. The total protein lysate was then collected by centrifugation at 4°C, 13,000 rpm for 1 hour. Fast protein liquid chromatography (FPLC) was utilized to purify his-tagged proteins from the whole cell

lysate. The purification process involved using a Ni-NTA column in the AKTA start system, and the his-tagged Cas13b protein was eluted using an imidazole elution buffer (20 mM sodium phosphate, 0.5 M NaCl, 500 mM imidazole, pH 7.4). Buffer exchange was carried out using the AKTA start system and a Hi-Trap Desalting column (5 ml). The proteins in the imidazole elution buffer were desalted in the Cas13b storage buffer. The Hi-Trap column was initially washed with 25 ml of filtered and degassed water at a flow rate of 5 ml/min, followed by equilibration with 1X storage buffer (50 mM Tris-HCl, pH 7.5, 600 mM NaCl, 2 mM DTT, and 10% glycerol). The flow rate was then decreased to 1 ml/min, and 1.5 ml of protein was manually applied to the column. Subsequently, 2 ml of buffer-exchanged protein was collected. Protein quantification was performed using the BCA assay (Thermo Fisher Scientific). BCA protein standards were prepared from a 2000 µg/ml BSA solution. The working reagent for the BCA assay was created by mixing Reagent A and Reagent B in a 50:1 ratio. 200 µl of this working solution was added to 10 µl of both standards and protein samples in a 96-well plate, using 10 µl of storage buffer as a blank. The plate was incubated for 30 minutes at 37°C in the dark. Absorbance was measured at 540 nm using a SpectraMax M5 Microplate Reader (Molecular Devices). Each measurement was performed in duplicates, and the average optical density (OD) of the standards was plotted against their concentrations. A standard curve was obtained, and the protein concentration of Cas13b was determined from the equation of the curve. Detailed process of Cas13b expression and purification is shown in Figure 3.

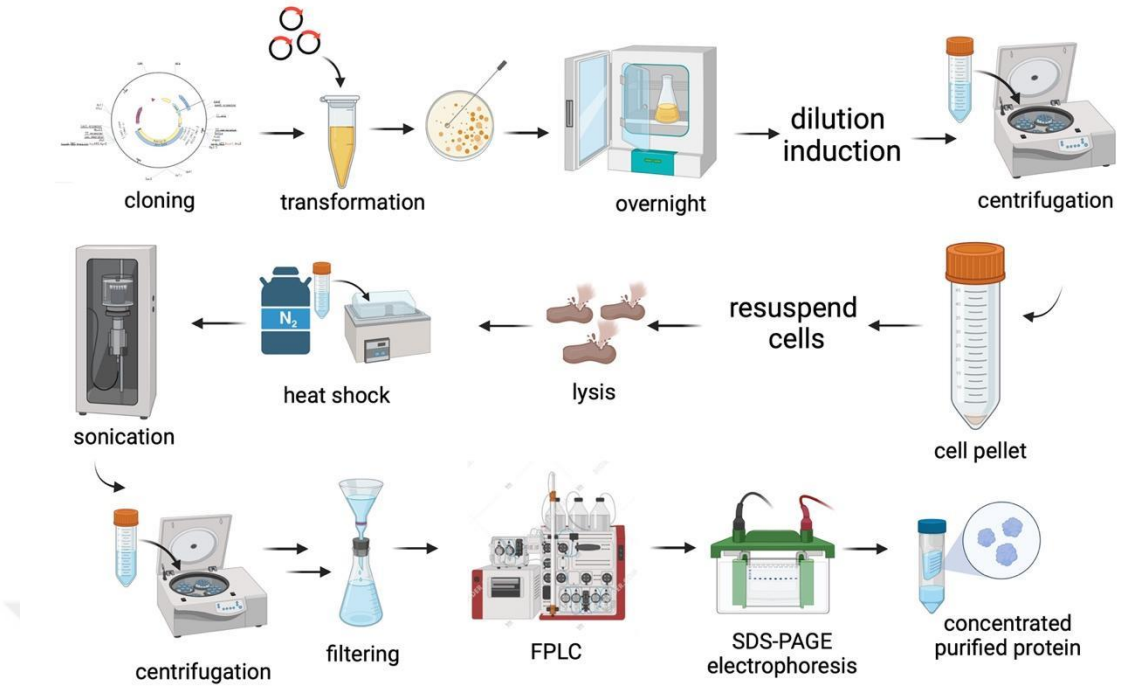

Figure 3: Expression and purification steps of Cas13b. Following transformation into *E. coli* cells, protein expression is induced. The cells undergo heat shock and sonication for lysis and release of the protein. Cas13b protein is then purified by FPLC and verified by SDS-PAGE electrophoresis. Illustration is created using BioRender.com.

2.7 SDS-PAGE of Cas13b Protein

SDS-PAGE (Sodium Dodecyl-Sulfate Polyacrylamide Gel Electrophoresis) analysis was conducted to determine the concentration of Cas13b post-buffer exchange. Twenty microliters of the purified and buffer-exchanged Cas13b protein, along with BSA standards (2 mg/mL, 1 mg/mL, and 0.5 mg/mL), were mixed with 4 µL of 6x SDS-PAGE loading dye. These samples were incubated at 95°C for 5 minutes before being loaded into 8% SDS-PAGE gel wells and run at 120V for 1.5 hours. After running, the gel was stained with Coomassie blue, heated in a microwave for 30 seconds, and then washed with distilled water. The gel was destained at room temperature until bands

appeared. Imaging and quantification of the bands were performed using a Chemidoc Imaging System (Bio-Rad) and ImageLab software (Bio-Rad).

2.8 *In Silico* gRNA Design

To design accurate gRNA for Cas13b activity, the target RNA sequence was identified and analyzed. The RNA sequence to be cleaved is from the Crimean-Congo hemorrhagic fever virus Turkey-Kelkit 06, Segment S (GenBank accession number: GQ337053.1). To target more than one strain simultaneously, this sequence was aligned with the Crimean-Congo hemorrhagic fever virus Ank2 isolate (GenBank accession number: MK309333.1). Both sequences were aligned using EMBOSS Needle to find homologous regions. For successful Cas13b-mediated knockout, a region within the RNA that is accessible and likely to be single-stranded was chosen as the target sequence using RNAfold.

The determined target RNA sequence was submitted to the CRISPR-RT tool to identify possible gRNA regions. Regions suggested by CRISPR-RT were double-checked with RNAfold to avoid strong secondary structures in the gRNA, which could inhibit Cas13b binding and nuclease activity. Finally, three candidate gRNA sequences (28 and 29 nucleotides long) were chosen to target the viral S segment RNA. The gRNA design was completed by adding a Direct Repeat sequence specific to RanCas13b of *Riemerella anatipestifer* species. This sequence is essential in the CRISPR-Cas13b system for forming the necessary secondary structure for crRNA processing and proper binding to the Cas13b enzyme. This enables crRNA maturation and ensures the enzyme's correct conformation for precise RNA targeting and cleavage.

2.9 *In vitro* Transcription (IVT) of gRNA and Target RNA

For the *in vitro* transcription (IVT) of the gRNA and target RNA, the HiScribe T7 High Yield RNA Synthesis Kit was used. The DNA sequence to be transcribed into gRNA was cloned into a plasmid under the T7 promoter earlier to enable IVT. As suggested by the manufacturer, the pET-22b-S1gRNA plasmid was digested with the EcoRI-HF (NEB) restriction enzyme at 37°C for 2 hours (digestion reaction protocol given in Appendix E, Table E.3). After digestion, a DNA template that is completely digested, free of supercoils, and free of RNA, protein molecules, and contaminants such as RNase and salts was obtained. The DNA sequence corresponding to the target RNA was received as the partial S segment genome of the CCHFV in the pcDNA™3.1-Segment.S plasmid from Ankara University Viral Zoonoses Advanced Research and Diagnostic Laboratory (AVZAL). This plasmid was obtained upon isolating viral RNA from cells followed by cDNA synthesis.

Primers were designed to amplify a 330-bp region corresponding to the target RNA while inserting bases for T7 promoter and T7 terminator regions. The digested DNA fragment corresponding to the gRNA plasmid and the 330 bp PCR product corresponding to the target RNA were loaded onto a 2% agarose gel containing SYBR™ Safe DNA gel stain for electrophoresis at 130V for 30 minutes. The respective expected bands on the agarose gel were cut out for DNA extraction by the Nucleospin Gel and PCR Clean-up Kit (Macherey-Nagel), following the manufacturer's instructions. The concentrations of extracted DNA were measured using the Thermo Scientific NanoDrop™ 2000 Spectrophotometer to determine the volume of the appropriate amount of DNA template for downstream IVT reactions.

The IVT reaction for both gRNA and target RNA was set according to the protocol for short RNA transcripts (<0.3 kb). A detailed protocol is provided in Appendix E, Table E11. The reaction mix was prepared in an RNase-free fume hood. The reaction was mixed thoroughly and incubated at 37°C for 16 hours. To remove template DNA, 20 µl of DNase I was added and incubated for 15 minutes at 37°C. The next step was to proceed with the purification of synthesized RNA transcripts using the Monarch RNA Cleanup Kit (NEB). Purification was carried out according to the manufacturer's guide. Four hundred microliters of RNA cleanup binding buffer was added to the IVT reaction, followed by the addition of 600 µl of ethanol (>95%). Then 900 µl of this mixture was loaded onto a column and centrifuged at 14,000 rpm for 1 minute. The flow-through was discarded, and the remaining IVT product was loaded onto the column. The column was then washed twice with 500 µl of RNA cleanup wash buffer, followed by a final spin to remove residual material. The IVT RNA was eluted with 60 µl of nuclease-free water. After a 3-minute incubation, the eluted sample was centrifuged at 14,000 rpm for 3 minutes. To prevent RNase degradation, 2.5 µl of Human Placenta RNase inhibitor was added to the eluted RNA.

Three microliters of each sample was taken for concentration analysis and gel electrophoresis to check the integrity of IVT products. The IVT RNA solutions were stored at -80°C until further use. Gel electrophoresis was performed in an RNase-free electrophoresis tank, cleaned with 70% ethanol and RNaseZAP solution. RNA products were mixed with 2X RNA loading dye in a 1:1 ratio, denatured at 70°C for 10 minutes, and incubated on ice for 2 minutes. Then the samples were loaded onto a 2% agarose-TBE (Tris-Borate-EDTA) gel (detailed recipe of TBE Buffer given in Appendix E, Table E.6) containing SYBR™ Safe stain for electrophoresis at 130V for 30 minutes.

Imaging and quantification of the bands were performed using a Chemidoc Imaging System (Bio-Rad) and ImageLab software (Bio-Rad).

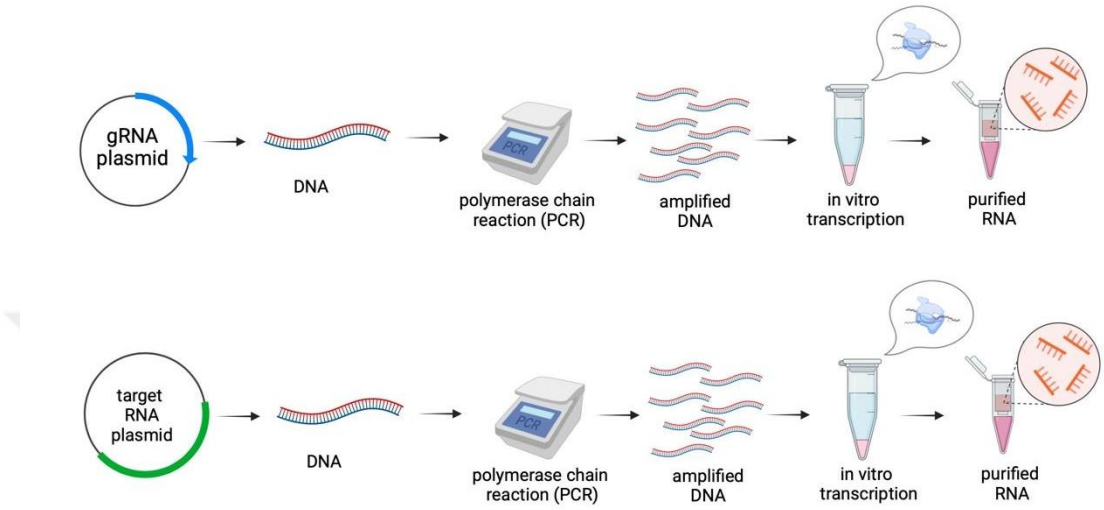

Figure 4: Figure 4: Schematic showing the IVT process. Template DNA for both RNA molecules is amplified for the IVT reaction. Illustration is created using BioRender.com.

2.10 *In vitro* RNA Cleavage Assay

To verify the Cas13b enzyme activity, an *in vitro* cleavage assay was designed (detailed recipe for the assay is given in Appendix E, Table E.13). Reaction buffer (recipe given in Appendix E, Table E.9 and E10), RNase inhibitor (human placenta, NEB), gRNA, and Cas13b were mixed on ice and incubated at 37°C for 20 minutes to allow ribonucleoprotein formation. Next, the target RNA was added, and the reaction mix was incubated at 37°C for 30 minutes. To stop the Cas13b activity, 2.5 µL of Proteinase K was added, and the sample was incubated at room temperature for 10 minutes. Reaction samples were mixed with 2X RNA loading dye in a 1:1 ratio, denatured at

70°C for 5 minutes, and incubated on ice for 2 minutes. The samples were then loaded onto a 2% agarose-TBE gel containing SYBR™ Safe stain for electrophoresis at 130V for 30 minutes. Imaging and quantification of the bands were performed using a Chemidoc Imaging System (Bio-Rad) and ImageLab software (Bio-Rad).

2.11 Maintenance of Mammalian Cell Line

The HEK293 (Human Embryonic Kidney 293) adherent cell line was utilized for CRISPR delivery via AAV due to several reasons: the presence of the Ad5 gene allows for high levels of recombinant protein production of proteins inserted into plasmid vectors containing the CMV promoter. The complete growth medium was prepared by mixing 445 ml of high glucose Reduced-Serum Medium (Opti-MEM™) with 50 ml of heat-inactivated Fetal Bovine Serum (FBS), and 5 ml of 100x Penicillin/Streptomycin. The media was filtered using a 0.45 μm sterile filter unit and stored at +4°C. To thaw HEK293 cells, complete Opti-MEM media was warmed in a 37°C water bath for 15 minutes prior to use. Cells were thawed in a 37°C water bath until only a small ice crystal remained. Thawed cells were transferred to a 15 ml conical centrifuge tube containing 5 ml of pre-warmed complete Opti-MEM media and centrifuged at 1500 rpm for 5 minutes. The supernatant was discarded, and the cell pellet was resuspended in 4 ml of complete Opti-MEM media and cultured in a T25 culture flask. The flasks were incubated in a CO_2 incubator set at 37°C with 5% CO_2. Cells were checked every other day under an inverted microscope to subculture when the confluency reached 80-90% (2-3 days). Subculturing involved discarding the media from the culture flask and washing cells gently with 5 ml of 1X PBS. They were detached from the flask using 1 ml of Trypsin-EDTA by incubating at 37°C for 2-3 minutes. Detached cells were transferred to a 15 ml tube and 4 ml of media was added to neutralize the toxic effects

of trypsin. Cells were centrifuged at 1500 rpm for 5 minutes. The supernatant was discarded, and the cell pellet was resuspended in 2 ml of fresh Opti-MEM media. Cells were seeded at 5x10^6 cells into a T75 culture flask.

2.12 Viral Transfection of HEK293 Cells

The transfection protocol for a 6-well plate using Lipofectamine® 3000 was performed by first seeding cells to achieve 70–90% confluency at the time of transfection. Lipofectamine® 3000 Reagent was diluted in two separate tubes, each containing a mixture of 125 µL of Opti-MEM® Medium and 5 µL of Lipofectamine 3000 reagent. A master mix was then prepared by diluting DNA in Opti-MEM® Medium and adding P3000™ Reagent, combining 250 µL of medium with 5 µg of DNA and 10 µL of P3000 reagent. The diluted DNA was added to each tube containing the diluted Lipofectamine® 3000 Reagent in a 1:1 ratio, mixing 125 µL of the diluted DNA (with P3000™ Reagent) with 125 µL of the diluted Lipofectamine® 3000 Reagent, and the mixture was incubated for 5 minutes at room temperature. Cells received 5 µg of pAAV-DJ vector, 5 µg of pHelper vector, and 5 µg of the Cas13b-L1gRNA pAAV expression vector. Next, 250 µL of the DNA-lipid complex was added to each well in a spiral manner and the cells were incubated for 2–4 days at 37°C before the transfected cells were analyzed.

During viral production, it was observed that some cells rounded up and detached, appearing to float in the medium, with viruses present in both the intact cells and the growth medium. To obtain a more concentrated virus stock, the cell pellet was processed. After 48-72 hours, 0.5 M Trypsin-EDTA was added to a final concentration of 10 mM to the plate and incubated for 3 minutes at room temperature, gently shaking the plate several times. All media, including cells, was then harvested into a sterile tube.

The mixture was centrifuged for 5 minutes at 3000 rpm to pellet the transfected cells, and the cell pellet was resuspended in 2.5 mL of serum-free DMEM. The cell suspension underwent four rounds of freeze/thaw cycles by alternating the tubes between a dry ice-ethanol bath and a 37°C water bath. The AAV supernatant was collected by centrifugation at 10,000g for 10 minutes, and the pellet was discarded. The viral supernatant was then stored at -80°C until purification.

2.13 Viral RNA Purification

Viral RNA was purified using the Nucleospin Dx Virus kit by Macherey-Nagel. A 200 µL sample containing the virus was lysed by adding 400 µL of Buffer RAV3. The mixture was vortexed vigorously for 15 seconds and incubated at room temperature for 5 minutes to ensure complete lysis. A NucleoSpin Dx Virus Column was placed in a Collection Tube, the lysate was loaded onto the column, and centrifuged at 11,000 x g for 1 minute. The flow-through was discarded, and the column was placed back into the Collection Tube. To wash the column, 500 µL of Buffer RAW was added to the column and centrifuged at 11,000 x g for 1 minute. The flow-through was discarded, and the column was placed back into the Collection Tube. Next, 600 µL of Buffer RAV3 was added to the column and centrifuged at 11,000 x g for 1 minute. The flow-through was discarded, and the column was placed back into the Collection Tube. Finally, 250 µL of Buffer RPE was added to the column and centrifuged at 11,000 x g for 2 minutes to dry the column. The flow-through and Collection Tube were discarded. The NucleoSpin Dx Virus Column was placed in a new 1.5 mL Elution Tube. To elute the viral RNA/DNA, 60 µL of RNase-free water was added directly to the center of the column membrane. The column was incubated at room temperature for 1 minute and

then centrifuged at 11,000 x g for 1 minute. The concentration of the viral RNA was measured using the Thermo Scientific NanoDrop™ 2000 Spectrophotometer.

CHAPTER III: RESULTS AND DISCUSSION

3.1 Cloning and Expression of Cas13b Protein

The gene circuit illustrated in Figure 5 was constructed using a pET-22b(+) vector available in our laboratory to express the Cas13b protein. This construct includes the RanCas13b gene, which is cloned under the T7 promoter. Protein expression is induced using IPTG, which activates the T7 promoter regulated by the Lac promoter. Following the gene, the MAPK NES (Mitogen-Activated Protein Kinase Nuclear Export Signal) sequence is included to regulate the subcellular localization of MAPKs and facilitate the export of Cas13b protein from the nucleus to the cytoplasm [60]. Additionally, a 6His (hexahistidine) Tag is present. This small tag does not interfere with the recombinant protein's function and structure but serves several purposes, such as improving solubility by aiding proper folding and preventing aggregation, enabling detection using an anti-His antibody in Western Blotting, and allowing affinity purification by binding Ni2+[61].

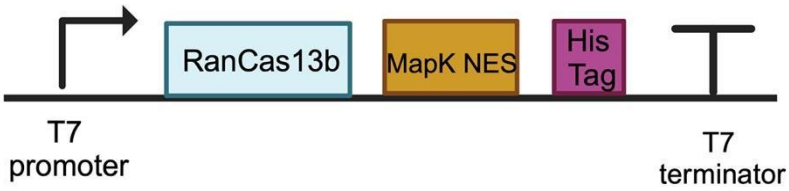

Figure 5: Schematic representation of Cas13b protein expressing construct. Cas13 protein was cloned under the T7 promoter followed by MAPK NES signal and His tag at C terminal. Illustration is created using BioRender.com.

To start, the Addgene plasmid #103855 was purchased. The RanCas13b region from this plasmid was amplified by PCR, resulting in an expected band of 3390 bases, as shown in Figure 6.

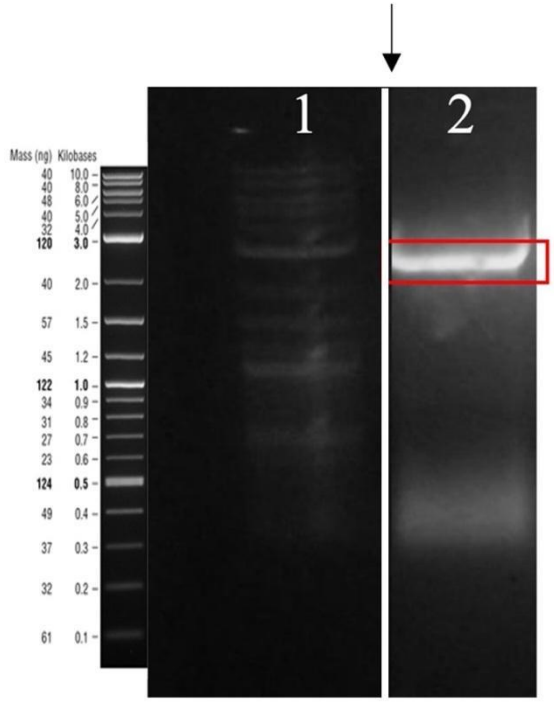

Figure 6: RanCas13b amplification. Agarose gel electrophoresis result of PCR-amplified 3390 bp RanCas13b (lane 2) from the Addgene plasmid. Lane 1 shows the DNA marker (NEB). The Cas13 gene was amplified to have overhang regions suitable for further Gibson assembly reaction. White line indicates the spliced agarose gel.

Next, the pET-22b(+)-GRFT-6His backbone was digested, and the expected band of approximately 5 kb, corresponding to the digested backbone, is shown in Figure 7.

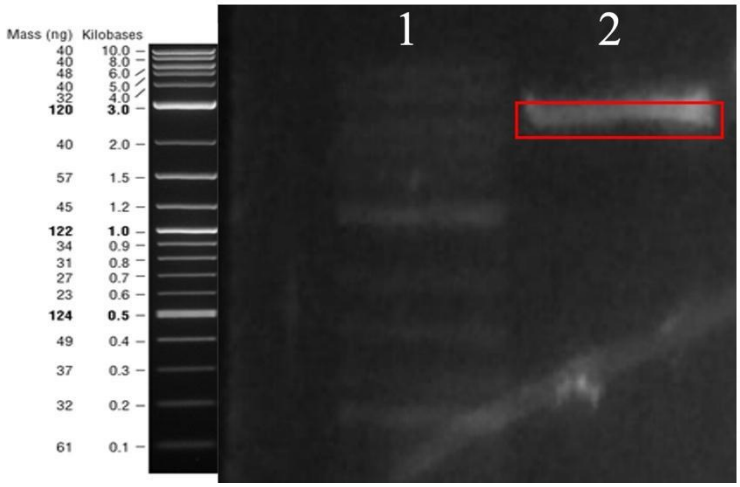

Figure 7: Cloning of the RanCas13 gene into the pET-22b(+) vector. Agarose gel electrophoresis result showing the pET-22b(+)-GRFT-6His backbone digested with XhoI (lane 2), resulting in a linear fragment of 5051 bases.

A Gibson assembly reaction was performed with the digested backbone and the PCR-amplified RanCas13b insert at a 1:1 molar ratio. The plasmid map of the resulting construct is provided in Figure C.1.

The pET-22b(+)-RanCas13b-6His plasmid was transformed into *E. coli* Rosetta and *E. coli* BL21 (DE3) cells for RanCas13b protein expression. Both strains, available in our laboratory, are deficient in Lon and OmpT proteases to reduce protein degradation, which is necessary for recombinant protein expression. Additionally, both strains contain the T7 promoter, allowing high-level expression of recombinant proteins when induced with IPTG [62]. However, some studies highlight the codon bias issue with BL21 cells, which lack rare tRNAs. This can pose a problem when expressing proteins with rare codons not found in the BL21 strain. In contrast, Rosetta cells do not have this issue due to the pRARE plasmid they carry [63].

To determine the best strain for Cas13b expression, both *E. coli* Rosetta and *E. coli* BL21 (DE3) cell types were transformed with the plasmid. Expression was induced when the OD600 of overnight-grown cells reached 0.4-0.6, using 1 mM IPTG at different temperatures and induction times to optimize the induction parameters. Table 2 lists the induction parameters tested. An 8% resolving gel was chosen to effectively resolve the 122 kDa Cas13b protein using SDS-PAGE and Western Blot. Figure 8 shows the SDS-PAGE gel image, and Figure 9 presents the Western Blot analysis of whole cell samples induced under the specified conditions. The highest protein expression was observed in BL21 cells induced at 30°C for 8 hours (Figure 9, lane 8). These conditions were selected for further Cas13b protein expression and purification.

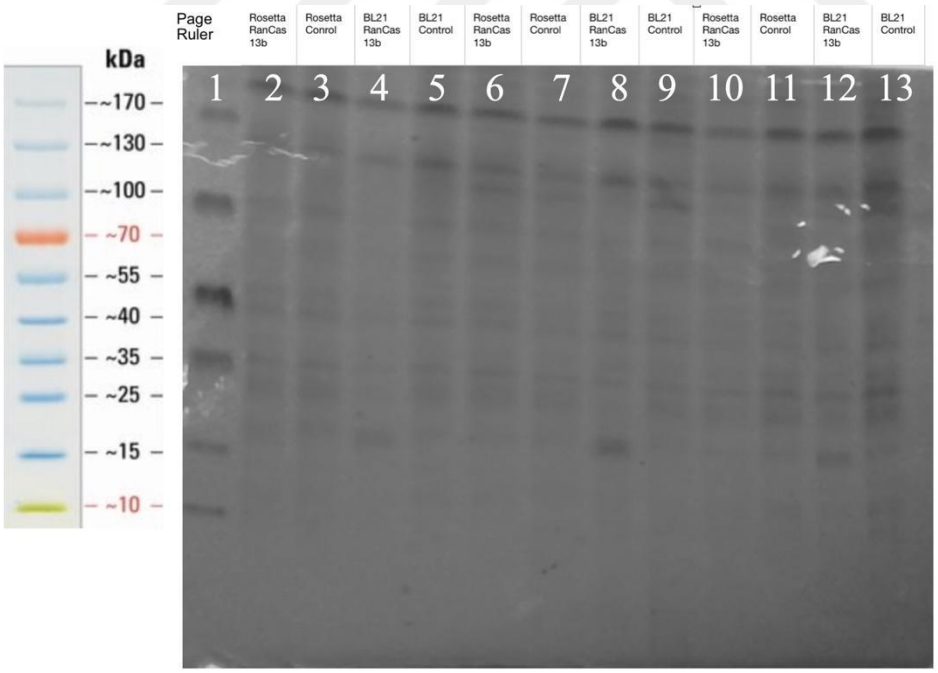

Figure 8: : SDS-PAGE verification of whole-cell samples. The first lane stands for the PageRuler ladder. Lanes 2, 6, and 10 are Rosetta RanCas13b cells; lanes 3, 7, and 11 are empty Rosetta control cells; lanes 4, 8, and 12 are BL21 RanCas13b cells; and lanes

5, 9, and 13 are empty BL21 control cells. Lanes 1-4 were induced at 37°C for 4 hours, lanes 5-8 were induced at 30°C for 8 hours, and lanes 9-13 were induced at 18°C for 16 hours with a final concentration of 1 mM IPTG.

Table 2: . 1 mM IPTG Induction Parameters Checked for Optimum Cas13b Expression

BL21 (DE3) Cells	37°C, 4 hours	30°C, 8 hours	18°C, 16 hours
Rosetta Cells	37°C, 4 hours	30°C, 8 hours	18°C, 16 hours

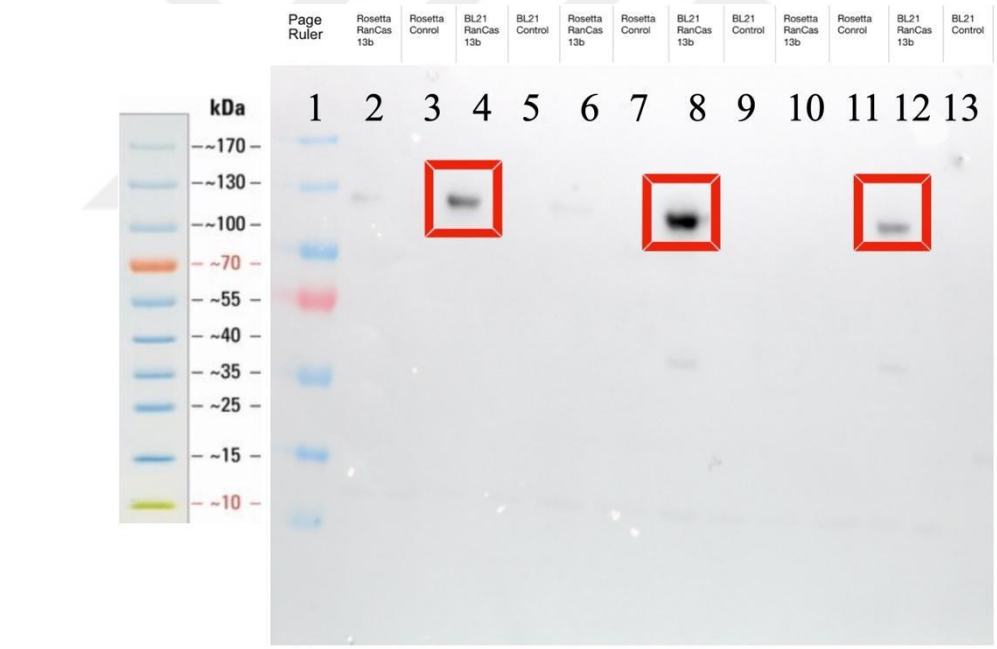

Figure 9: Western blot image of whole-cell samples induced with 1 mM IPTG under different conditions. The first lane represents the PageRuler ladder. Lanes 2, 6, and 10 are Rosetta RanCas13b cells; lanes 3, 7, and 11 are empty Rosetta control cells; lanes 4, 8, and 12 are BL21 RanCas13b cells; and lanes 5, 9, and 13 are empty BL21 control

cells. Lanes 1-4 were induced at 37°C for 4 hours, lanes 5-8 were induced at 30°C for 8 hours, and lanes 9-13 were induced at 18°C for 16 hours.

Once the optimal induction parameters and host strain were determined, Cas13b was expressed in BL21-RanCas13b cells by induction at 30°C for 8 hours. Following incubation, the cells were prepared for protein purification. Detailed steps and buffer recipes are described in section 2.4. A Ni-NTA column was selected for purification as it utilizes the affinity of histidine residues for nickel ions. The histidine tag in the construct allows interaction between the imidazole rings of histidine residues and the nickel ions. Multiple coordination bonds between these entities ensure effective purification [64]. This interaction is reversible, enabling the elution of the desired protein at the end of the purification protocol.

Apart from the nickel ions, the Ni-NTA resin contains NTA (nitrilotriacetic acid) as the chelating agent to support Ni2+-histidine interactions over its four coordination sites [65]. This specific interaction leads to the separation of His-tagged Cas13b proteins from other proteins of the *E. coli* cells. The imidazole concentration is adjusted in three buffers (binding buffer, wash buffer, elution buffer) used in the FPLC process. Imidazole inherently competes with the histidine residues for resin binding, ensuring the washing away of non-specific proteins for selective elution. As described in section 2.4, imidazole was removed, and the protein sample was transferred into a storage buffer to ensure high purity of Cas13b protein for downstream applications. Following successful protein purification via FPLC, all sample fractions, as well as the whole cell lysate, were analyzed by SDS-PAGE as shown in Figure 10.

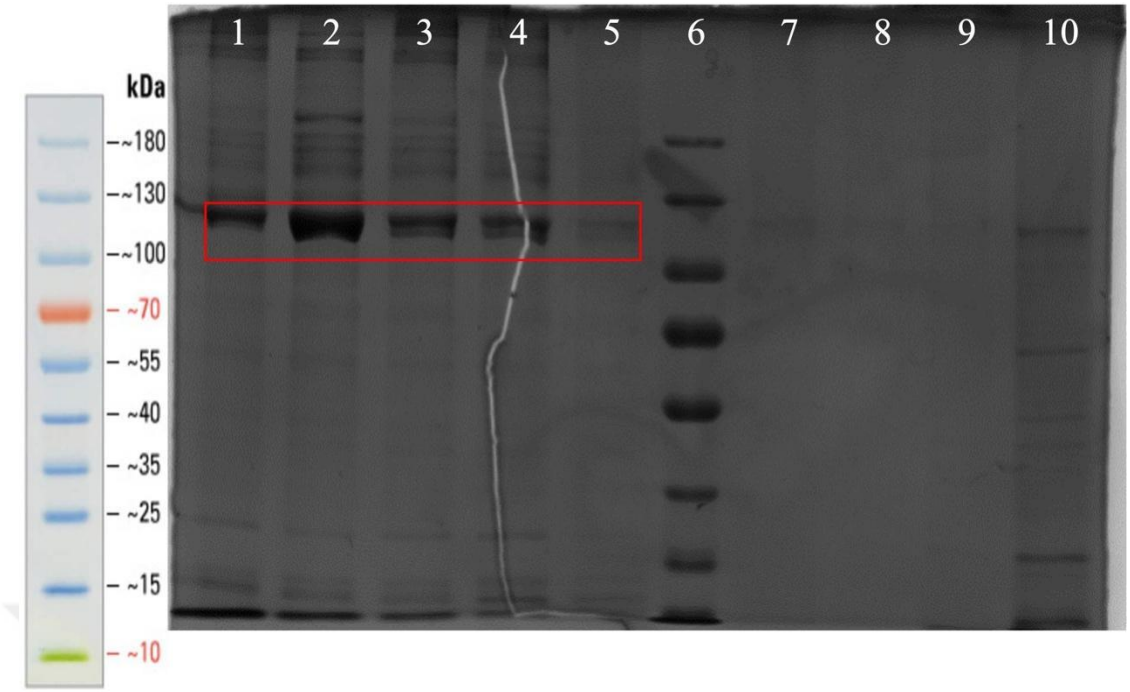

Figure 10: SDS-PAGE analysis of Cas13 protein. Lane 6 represents the PageRuler ladder. Lanes 1-4 and 7-9 are the FPLC fractions. Lane 10 is the whole-cell lysate. Lane 2 shows the highest protein concentration, indicated by the thickest band corresponding to the 122 kDa Cas13 protein.

3.2 *In Silico* gRNA Design

Cas13b exerts RNA-guided RNase activity to cleave single-stranded RNA (ssRNA) sequences. The enzyme activity is directed by the gRNA through its spacer sequence, which matches the target RNA sequence along with the direct repeat sequence. Before designing the gRNA, the target region was determined. Two strains were selected for targeting, with their GenBank accession numbers provided in section 2.7. The sequences of these strains were aligned using EMBOSS Needle to identify homologous regions, thereby increasing the likelihood of RNA knockdown. The sequence alignment is depicted in Figure 11.

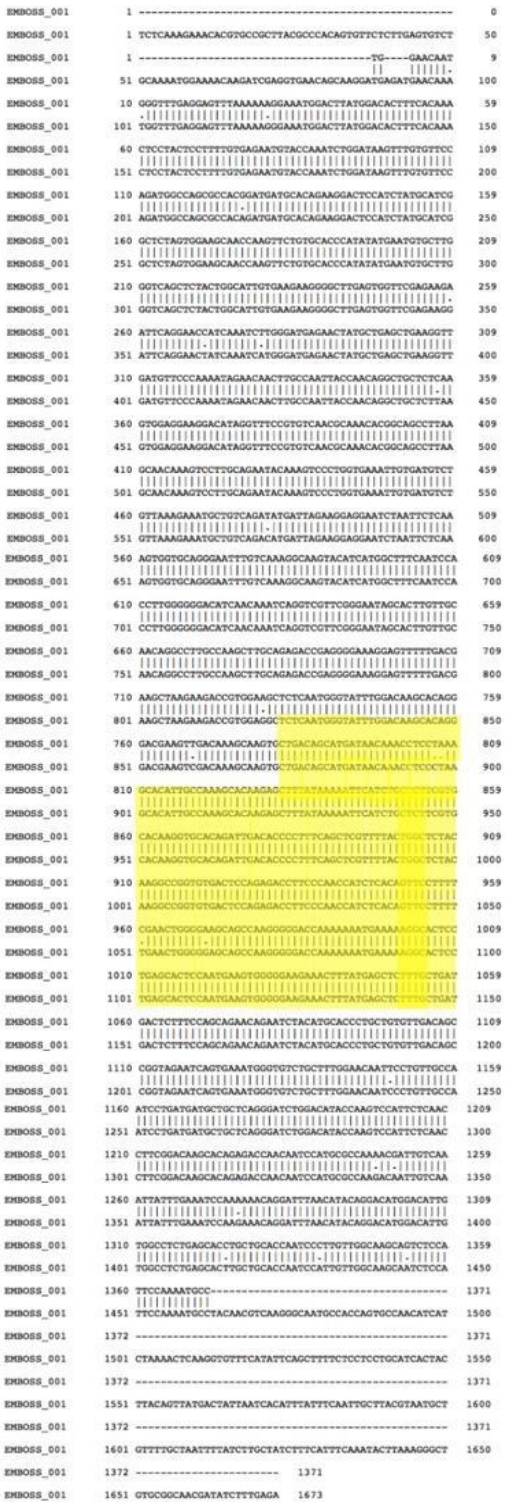

Figure 11: Homology search using EMBOSS Needle tool between the Crimean-Congo hemorrhagic fever virus Turkey-Kelkit 06, Segment S (GenBank accession number: GQ337053.1) and Crimean-Congo hemorrhagic fever virus Ank2 isolate (GenBank

accession number: MK309333.1) sequences. The 330-bp region selected as the target is highlighted in yellow.

The homologous region identified by the tool was analyzed for possible stable secondary structures that could block enzyme activity. Using RNAfold, the secondary structure of the target RNA region was predicted. RNAfold calculates the minimum free energy (MFE) configuration of the RNA sequence to show secondary structures such as hairpins, stems, and loops. Figure 12 describes the secondary structure output given by RNAfold in both dot-bracket notation and graphical output, along with the MFE values of the aligned sequences. Lower MFE values indicate stable secondary structures that should be avoided, whereas higher MFE values suggest a lower likelihood of secondary structure formation.

Figure 12: The secondary structure analysis of target RNA. Output given by RNAfold is shown in graphical output on the left and in the dot-bracket notation on the right for the Crimean-Congo hemorrhagic fever virus Turkey-Kelkit 06, Segment S (GenBank accession number: GQ337053.1) genome sequence.

In the left panel of Figure 12, regions depicted in loops and single-stranded regions correspond to higher MFE values. Panel right provides a graphical output with color codes: red indicates a very high base pairing probability (close to 1), orange/yellow

indicates high to moderate base pairing probability, green stands for moderate base pairing probability, cyan/light blue represents a lower base pairing probability, and blue depicts a very low base pairing probability (close to 0).

Accordingly, a 330-bp long region that is homologous and free of secondary structures was chosen as the target RNA region. The next step was the gRNA design. The Cas13b enzyme does not require a PAM sequence. The gRNA for this enzyme is a combination of a direct repeat (DR) sequence, which forms the unique hairpin structure, and the spacer region, which is complementary to the target sequence. The DR is specific to the Cas enzyme variant and was obtained from the literature.

To generate complementary gRNA spacer sequences, the target RNA sequence was input into the CRISPR-RT tool. This *in silico* gRNA design tool works by scoring based on specificity (to minimize off-target effects), efficiency (to assess how effectively the gRNA would guide the Cas13b enzyme in RNA targeting), and secondary structure (to ensure the gRNA is free of secondary structures and accessible). The three highest-scoring candidates were selected and further analyzed with RNAfold to double-check for secondary structures. Figure 13 shows the sequence and RNAfold analysis results for the gRNA selected among the three candidates to target a 330-bp region in the viral S segment RNA.

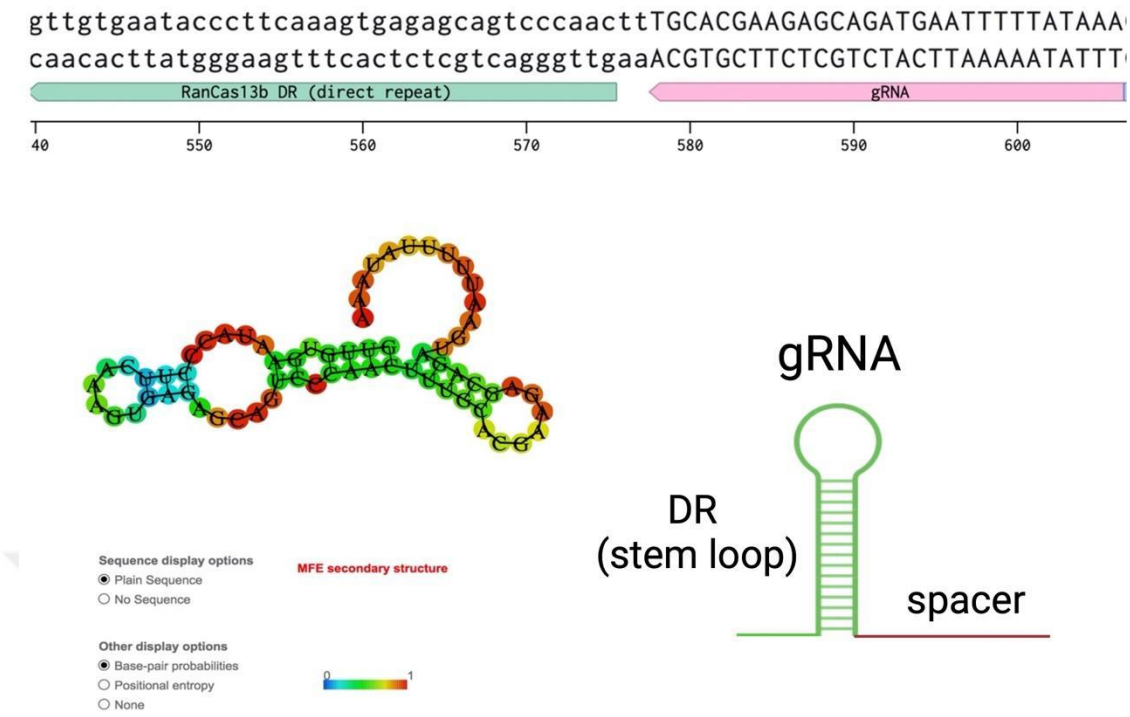

Figure 13: RNAfold analysis of gRNA. Final sequence and the secondary structure of the gRNA designed to target the viral S segment genome. The final gRNA is composed of two parts: the direct repeat sequence forming the stem loop and the spacer sequence complementary to the target RNA sequence.

3.3 gRNA and Target RNA Production by IVT

The DNA template for the IVT reaction of the target RNA was obtained in the pcDNA™3.1-Segment.S plasmid from Ankara University Viral Zoonoses Advanced Research and Diagnostic Laboratory (AVZAL). Primers EA13 and EA14 were designed to amplify a 330-bp region corresponding to the target RNA while inserting bases for the T7 promoter and T7 terminator regions. The DNA sequence to be transcribed into gRNA was cloned into a pET-22b plasmid under the T7 promoter, as shown in Figure 14, using primers EA3 and EA4 listed in Appendix B.

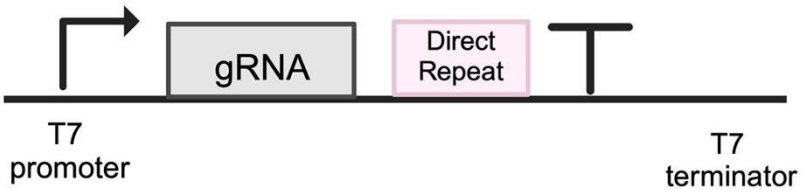

Figure 14: Schematic representation of the pET22B-S1-gRNA construct with the gRNA and DR sequences under the T7 promoter.

The resulting construct was loaded onto an agarose gel, and the band was observed at 5283 bases, as depicted in Figure 15. The plasmid was later sent for NGS sequencing.

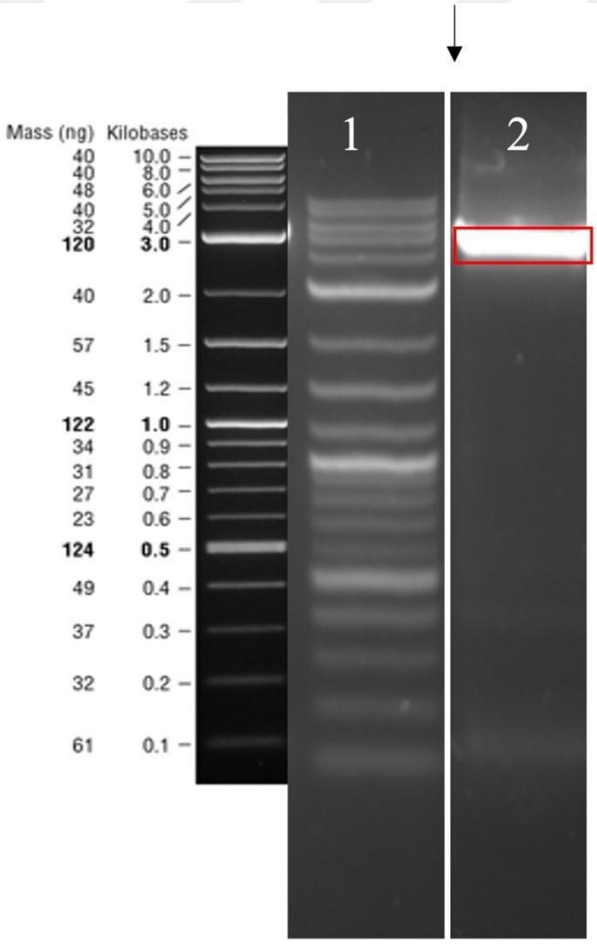

Figure 15: The pET-22b backbone was amplified by primers incorporating gRNA and DR sequences, with an expected band size of 5280 bases. White line indicates the spliced agarose gel.

The plasmid was then digested to obtain a linear DNA template necessary for the IVT reaction, as shown in Figure 16. Both linear DNA fragments were subjected to the IVT reaction. The IVT product of target RNA is shown in Figure 16; however, the IVT product of gRNA was not observed on the agarose gel, probably due to its small size of 68 bp.

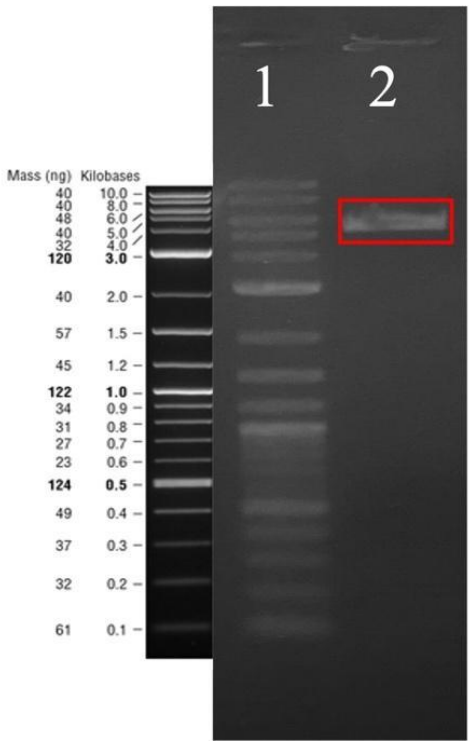

Figure 16: pET-22b(+)-gRNA-S backbone digestion.

3.4 *In vitro* Cleavage Assay

There are several key points to consider when designing an *in vitro* cleavage assay. As described in section 2.10, the main reaction components are gRNA, target RNA, and the Cas13b enzyme. An appropriate reaction buffer must be prepared to assemble all reaction components. Figure 17 shows the initial cleavage reaction data. This initial cleavage reaction was set up using the commercial CutSmart Buffer (NEB). At the time of designing this assay, no detailed digestion protocol was available for the Cas13b enzyme used in this study. Therefore, the reaction buffer, reaction duration, and the

amount of each component were adjusted multiple times to determine the optimal reaction parameters.

The reaction was set up in an RNase-free biological safety cabinet using RNase-free pipette tips and equipment to prevent RNA degradation. A mixture of 10X CutSmart buffer, RNAse inhibitor (human placenta, NEB), gRNA, and Cas13b was prepared on ice and incubated at 37°C for 20 minutes to allow ribonucleoprotein formation. Next, the target RNA was added, and the reaction mix was incubated at 37°C. To stop the Cas13b activity, 2.5 µl Proteinase K was added, and the sample was incubated at room temperature for 10 minutes. The resulting mix was loaded onto a 2% agarose-TBE gel for further analysis as explained in section 2.10.

Various parameters were tested in this reaction. Inspired by the protocol for *in vitro* Cas12 digestion, the final concentrations of each component were determined as follows: 30 nM gRNA, 30 nM Cas13b, and 3 nM target RNA [66]. The known molecular weight (grams/mol) of each molecule was converted to µg per µmol. The molecular weight of gRNA and target RNA was calculated based on size, and for Cas13b, it was obtained from the literature. The concentration given in µM was then multiplied by the molecular weight in micrograms per micromole to obtain the concentration in micrograms per microliter. Based on the measured concentrations of each sample, the volume needed to reach the desired nM final concentration was calculated.

Figure 17 shows the absence of the 330-bp band corresponding to target RNA in lanes 4, 5, 6, and 7, indicating RNA degradation by Cas13b.

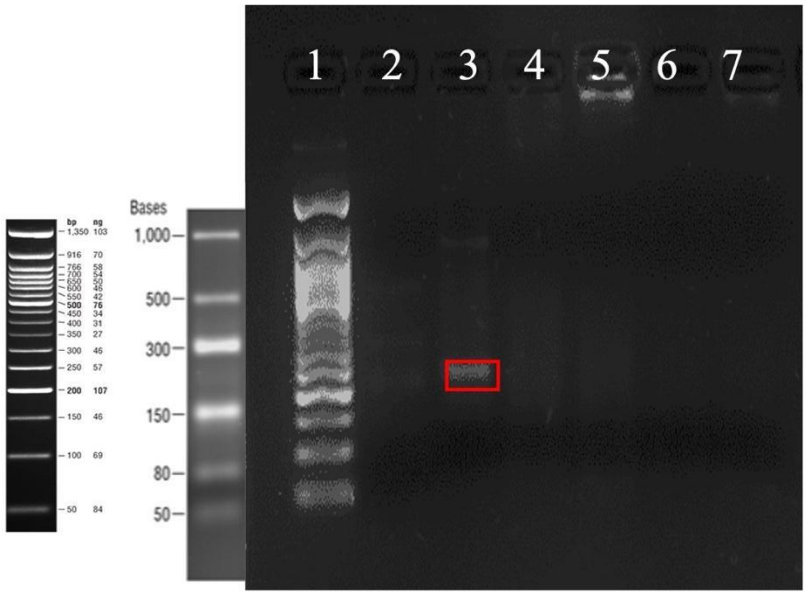

Figure 17: *In vitro* cleavage assay with CutSmart (NEB) buffer. Showing the target RNA degradation by guided Cas13 enzyme activity. Reaction conditions for all lanes are given in Table 3. Lanes 4 and 6 show that the target RNA was successfully cleaved, as the band corresponding to 300 bp is missing. Lane 1 shows the dsDNA marker, and lane 2 shows the ssRNA marker. The RNA marker is barely visible; however, it is clear that the bands of both markers are almost in parallel. The bands of the DNA marker are slightly above those corresponding to the RNA marker of the same size, due to DNA molecules being heavier as they are double-stranded. Therefore, in following experiments, this was kept in mind and a DNA ladder was utilized for better visibility.

Table 3 shows the amount of each molecule used in the reaction. Lanes 5 and 7, which included 30 nM Cas13b, 30 nM gRNA, and 3 nM target RNA, show some of the sample left in the wells, in contrast to lanes 4 and 6, which included 10 nM Cas13b, 10 nM gRNA, and 1 nM target RNA. This was likely due to the excessive amount of Cas13b added to the reaction, making 30 nM Cas13b too heavy to run on the gel. Therefore, it can be concluded that the samples loaded in lanes 4 and 6 ran completely on the gel, and the target RNA was degraded by the guided Cas13b enzyme. The reaction samples

in lanes 5 and 7 were incubated for 1 hour, while those in lanes 4 and 6 were incubated for 30 minutes. Thus, 30 minutes seems sufficient for RNA degradation by Cas13b.

Table 3: . *In vitro* Cleavage Assay Reaction Conditions

Lane	Cas13b	gRNA	Target RNA	Reaction duration
4	10 nM	10 nM	1 nM	30 minutes
5	30 nM	30 nM	3 nM	1 hour
6	10 nM	10 nM	1 nM	30 minutes
7	30 nM	30 nM	3 nM	1 hour

After the optimum reaction duration and the amount of each reaction component were determined, a specific reaction buffer for Cas13b was prepared. According to the literature, an *in vitro* reaction for Cas13b has not yet been established. Therefore, two candidate buffers with useful ingredients were prepared, with their recipes given in Appendix E, Table E.9 and E.10.

The reaction buffer A includes HEPES (4-(2-hydroxyethyl)-1-piperazineethanesulfonic acid) at pH 7.0, KCl, 2 mM MgCl2, DTT (dithiothreitol) , and glycerol. Here, HEPES is a zwitterionic buffer providing buffering capacity in the physiological pH range, KCl is a salt that stabilizes the reaction environment by providing ionic strength, MgCl2 is an essential cofactor for nuclease activity, DTT (dithiothreitol) is used as a reducing agent to keep Cas13b in a reduced state for improved nuclease activity, and glycerol provides a stable environment [67–70].

The reaction buffer B includes Tris-HCl at pH 7.5, NaCl, 0.5 mM MgCl2, DTT, and BSA (bovine serum albumin). Here, the pH of the buffer B is slightly more alkaline, the concentration of MgCl2 is lower than in the buffer A, and BSA replaces glycerol to

stabilize enzyme activity and prevent nonspecific interactions. Both buffers were tested to determine the appropriate reaction buffer in terms of optimal pH for Cas13b activity and other conditions. Figure 18 shows data for *in vitro* cleavage reactions set up using both buffers. Enzyme activity appears much better in Figure 18A, where the reaction was set up using the buffer A containing HEPES. Here, the 330-bp long target RNA was cleaved into two pieces observed in lane 4, as the 330 bp band went missing as it was cleaved to two pieces at 230 bp and 100 bp. According to this data, it can be stated that *in vitro* Cas13b activity is visible when a reaction is set up using 10 nM Cas13b, 10 nM gRNA, and 1 nM target RNA at 37°C for 30 minutes in the reaction buffer A.

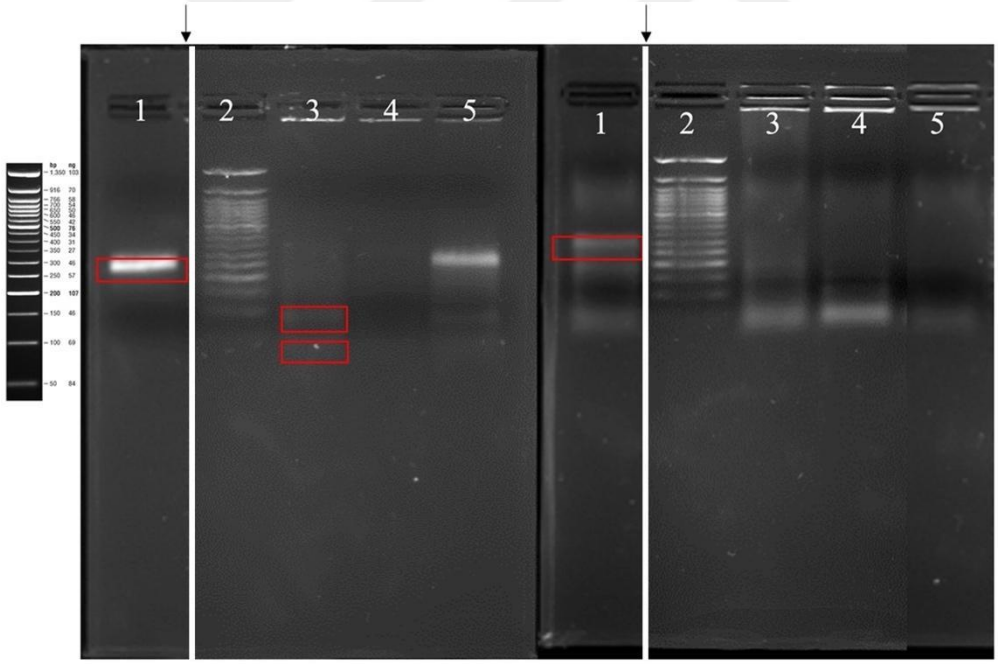

Figure 18: *In vitro* cleavage assay with homemade reaction buffers. On the left, cleavage assay was set up in reaction Buffer A. On the right, cleavage assay was set up in reaction Buffer B. Both of the gel images show target RNA of 330 bp in the first lane, lane 2 shows DNA marker. Lane 3 and 4 shows 10 nM Cas13b, 10 nM gRNA and 1 nM target RNA. Lane 5 shows 30 nM Cas13b, 30 nM gRNA and 3 nM target RNA.

The reaction samples in lane 3 and 5 were incubated for 30 minutes, the sample in lane 4 was incubated for 1 hour. White lines indicate the spliced agarose gel.

3.5 Cloning of pAAV-Cas13b-gRNA-L

The gene circuit shown in Figure 19 was constructed in the pAAV-MCS vector purchased from CellBiolabs. The construct includes the RanCas13b gene and the U6 cassette expressing gRNA and DR necessary for Cas13b activity. The U6 promoter has been effectively utilized for expressing guide RNA (gRNA) in the CRISPR-Cas13b system similar to its use in CRISPR-Cas9 systems [41,71]. This promoter is particularly favored due to its strong transcriptional activity, which is crucial for generating the high levels of gRNA required for efficient RNA targeting and cleavage by Cas13b effectors. The U6 promoter's robust, continuous expression and compatibility with RNA polymerase III make it an ideal choice for driving gRNA expression in CRISPR systems [72].

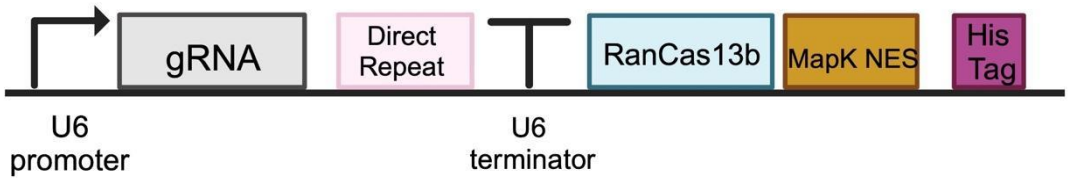

Figure 19: Schematic representation of the final pAAV-Cas13-gRNA-L construct.

To start, the RanCas13b region in the pET-22b(+)-Cas13b-6His backbone was amplified by PCR using primers EA5 and EA6 listed in Table B.1 and the Q5 polymerase. The amplified RanCas13b PCR product, as well as the pAAV backbone, were double-digested. All products from the three digestion reactions were loaded onto an agarose gel, as shown in Figure 20.

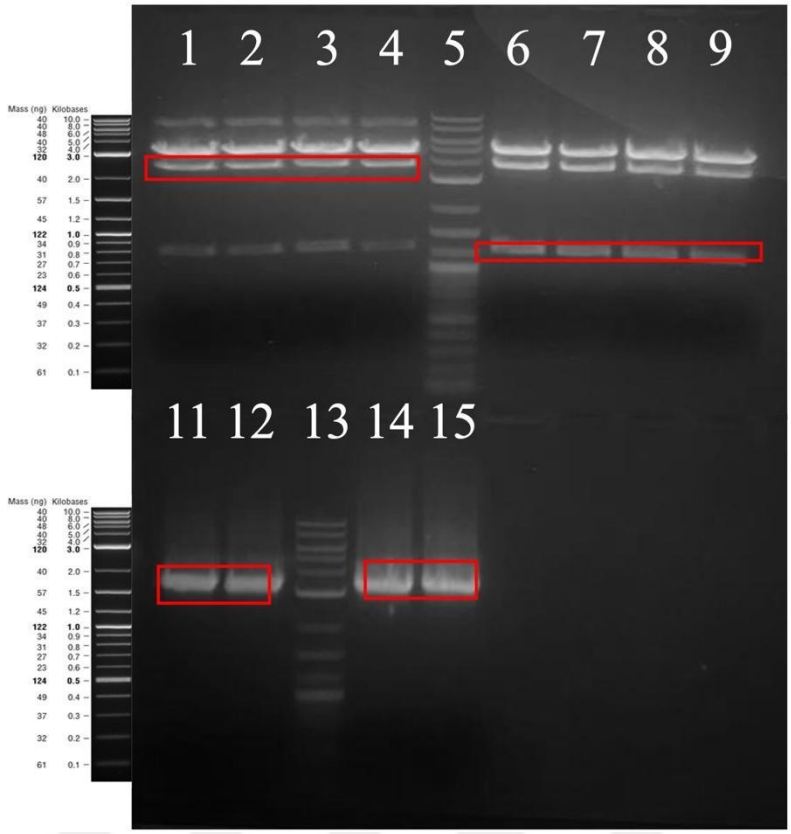

Figure 20: PCR result for three digestion reactions. Lanes 1-4 show pAAV-MCS backbone digested with Mlu1-HF and HindIII enzymes. The larger fragment of this digestion corresponding to 3.4kb was extracted. Lane 5 was loaded with 1kb plus DNA marker (NEB). Lanes 6-9 show pAAV-MCS backbone digested with Mlu1-HF and EcoRI enzymes. The smaller fragment of this digestion corresponding to 1.2 kb was digested. Lanes 11, 12, 14, 15 show the Cas13 PCR product amplified from pET-22b(+)-GRFT-6His backbone and digested with EcoRI and HindIII enzymes. The expected band at 3387 bp is shown.

Since all three DNA fragments had matching ends, they were ligated using T4 ligase (detailed recipe given in Appendix E, Table E.8). The three fragments were ligated as follows: 50 ng larger pAAV digest fragment (3.4 kb), 50 ng smaller pAAV digest fragment (1.2 kb), and 100 ng Cas13b insert (3.4 kb). The ligated plasmid of 8 kb was then transformed into *E. coli* DH5α cells and plasmid DNA were isolated for digestion

verification. Figure 21 shows the double digestion verification and the expected bands of 3.4 and 4.6 kb.

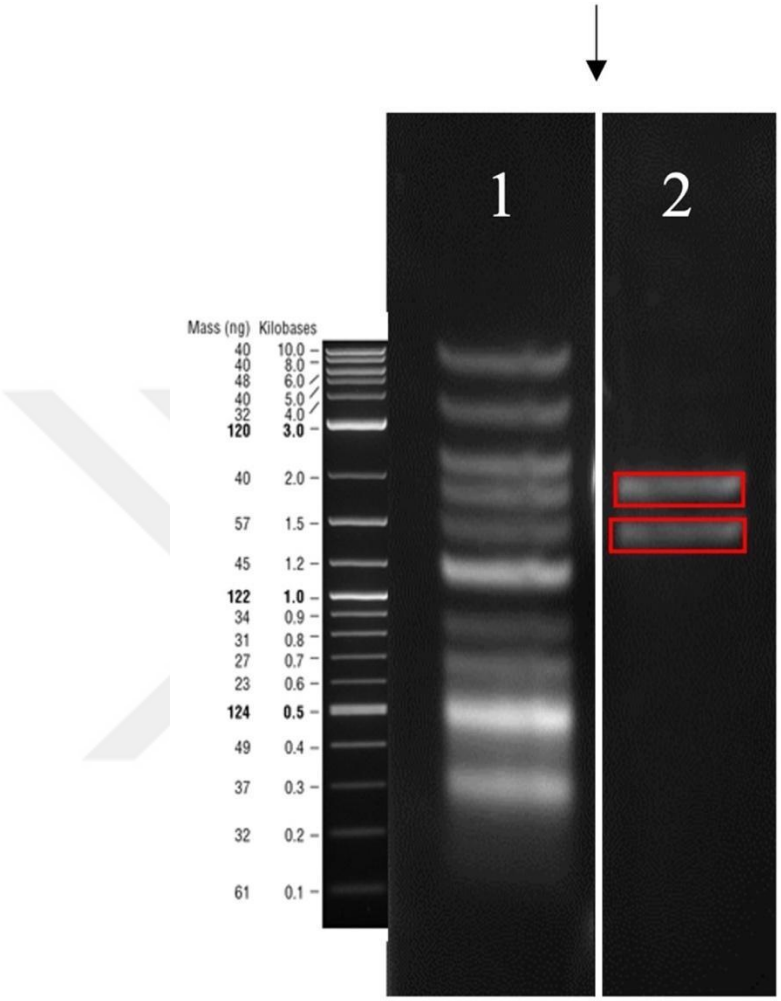

Figure 21: : Double digestion verification of the pAAV-Cas13 plasmid. The expected digest products are 4.6 kb and 3.4 kb. White line indicates the spliced agarose gel.

The next step was to clone the gRNA and DR regions into the verified pAAV-Cas13b plasmid. Cloning was done in two consecutive PCR reactions using the primers EA7, EA8, EA9, and EA10 listed in Appendix B. The template for the first PCR reaction was the Addgene #78741 plasmid containing the U6 cassette for gRNA cloning. Figure 22 shows the PCR products of the first and second rounds of PCR, where the DNA product from the first PCR, extracted from the gel, was used as the template for the second PCR.

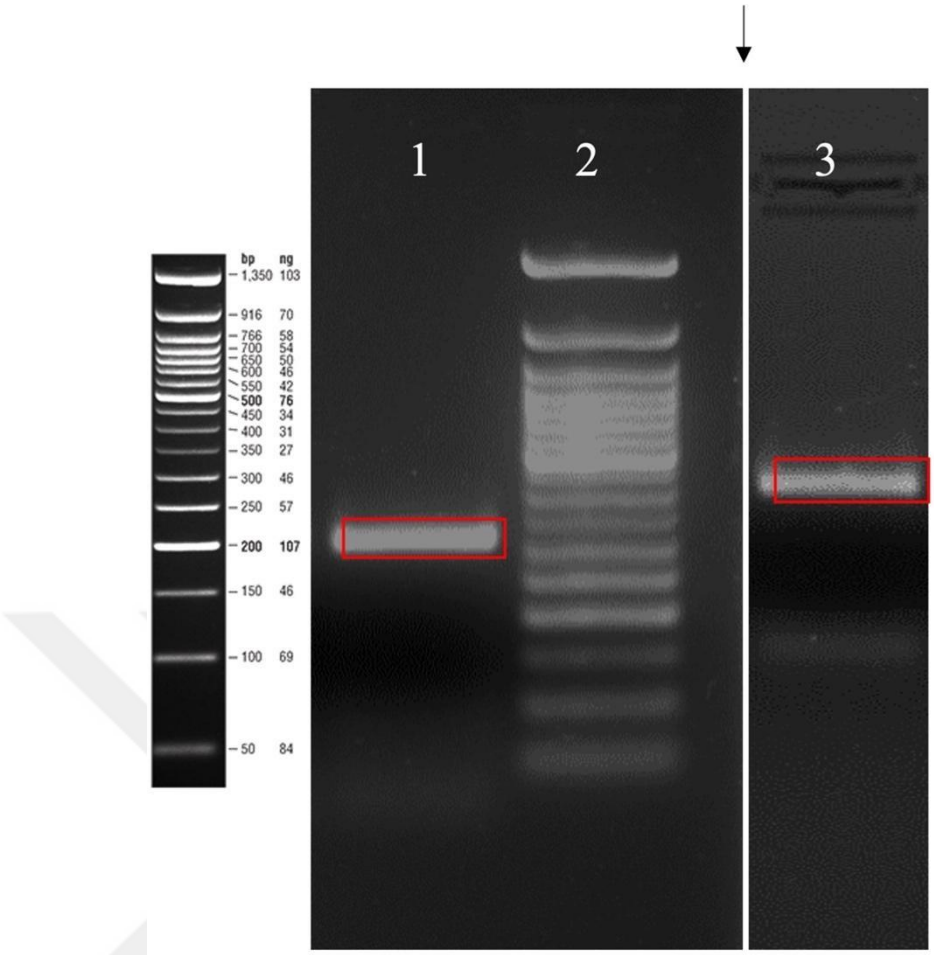

Figure 22: Cloning by PCR of the U6 cassette. Lane 1 shows the 286 bp PCR product from the first round of PCR, Lane 2 shows the DNA marker (NEB), and Lane 3 shows the 380 bp product from the second round of PCR. White line indicates the spliced agarose gel.

After DNA extraction, the U6 cassette was incorporated into the single digested pAAV-Cas13b backbone using Gibson assembly. The single digestion of the pAAV-Cas13b is shown in Figure 23. The Gibson assembly product was then transformed into *E. coli* DH5α cells, and plasmid DNA was isolated for Sanger sequencing verification.

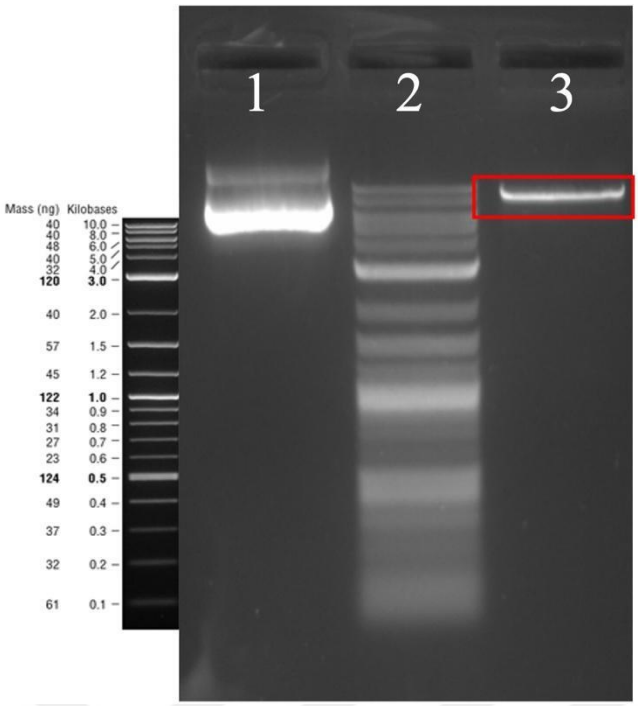

Figure 23: Digestion of the pAAV-Cas13 backbone. The circular plasmid is shown in Lane 1, Lane 2 shows the DNA marker (NEB), and the linear digest product is shown in Lane 3.

3.6 rAAV Mediated Delivery of CRISPR/Cas13b System into HEK293 Cells

To demonstrate the inhibition of CCHFV replication in HEK293 cells via the CRISPR/Cas13b system, a gene delivery agent is required. For this purpose, the versatile rAAV (recombinant adeno-associated virus) was selected due to its numerous advantages. AAV vectors have a high efficiency of transduction, ensuring that a higher percentage of HEK293 cells will receive the CRISPR/Cas13b system components. These vectors are much safer than adenovirus and lentivirus as they are known to elicit minimal cytogenic effects and low immunogenicity [73]. Additionally, AAV vectors provide long-term gene expression without incorporating into the host genome, ensuring sustained RNAse activity [74].

The AAV-DJ Helper Free Packaging System was purchased from CellBiolabs for this purpose. The system is composed of three components: the expression vector carrying the CRISPR/Cas13b agents, the pHelper vector, and pAAV-DJ. The pHelper plasmid supplies the Adeno E2A, E4, and VA RNA genes necessary for AAV production. Other necessary genes are supplied by HEK293 cells stably expressing the adenovirus E1 gene. The pAAV-DJ plasmid provides the rep and cap genes responsible for AAV replication and packaging in the host cells [75].

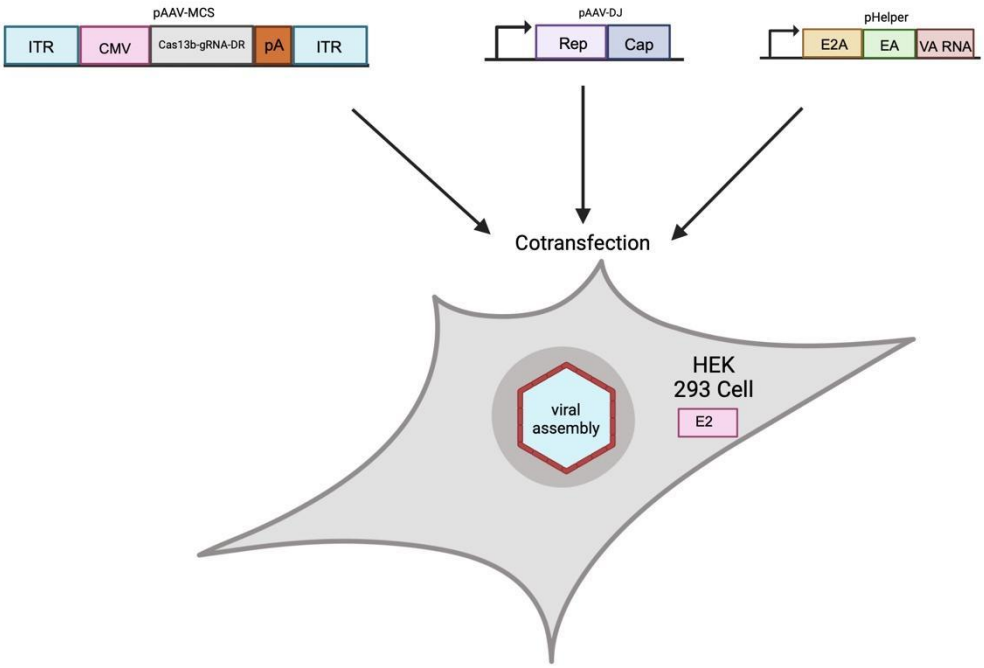

Figure 24: The three plasmid components of the AAV gene delivery system.

Cas13b and gRNA were cloned into the pAAV plasmid as described in section 3.5. After cloning, the three components of the AAV delivery system were cotransfected into HEK293 cells, as detailed in section 2.11 and llustrated in Figure 24. If the CRISPR agents are successfully transfected into the HEK293 cells, the AAV-specific genes should be expressed from the supplied plasmids, leading to replication of the AAV

vector DNA carrying CRISPR agents within the cells, followed by packaging of the replicated AAV vector DNA into capsids to form mature AAV particles as illustrated in Figure 25 [76].

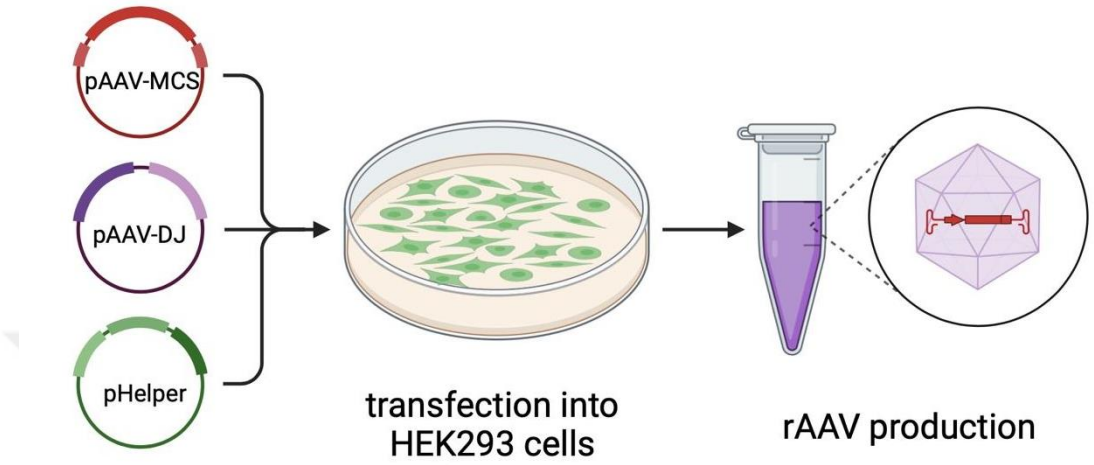

Figure 25: : The workflow of rAAV production in HEK293 cells.

To gather initial data on the successful delivery and packaging of the system, a PCR reaction was set up. Figure 26 shows the agarose gel image of the PCR reaction. This figure displays the band corresponding to the Cas13b gene amplified by primers EA11 and EA12 given in Appendix B. It is concluded that the HEK293 cells express the vector plasmid carrying the CRISPR/Cas13b agents, including the Cas13b gene and the corresponding gRNA.

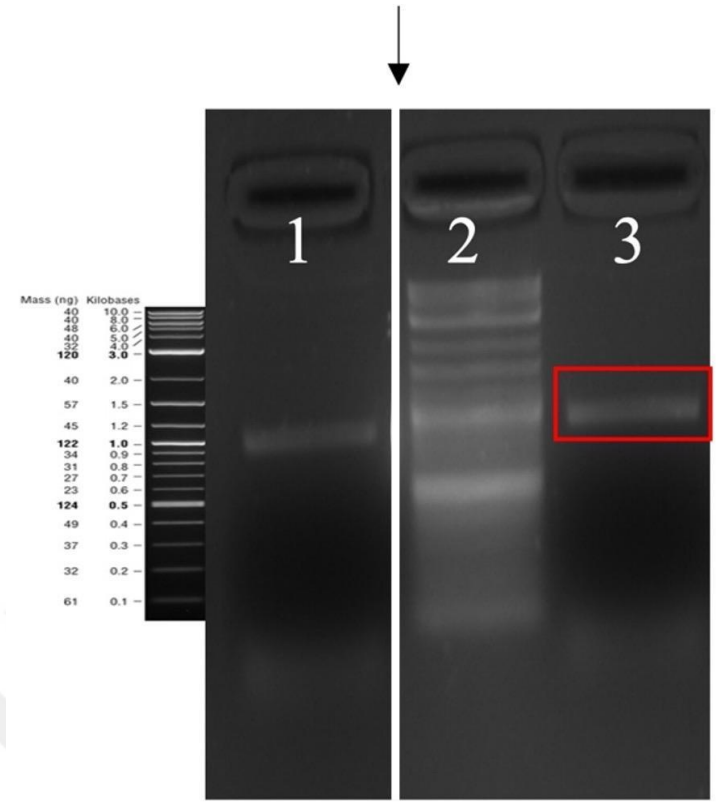

Figure 26: PCR reaction to verify the delivery and packaging of the CRISPR/Cas13b system. The 870 bp region of the Cas13b gene sequence was amplified. Lane 1 shows the pET-22b(+)-Cas13b-6His plasmid loaded as a positive control, Lane 2 shows the DNA marker (NEB), and Lane 3 shows viral DNA isolated from the HEK293 cell supernatant. White line indicates the spliced agarose gel.

CHAPTER IV: CONCLUSION

In this project, we aimed to combat Crimean-Congo Hemorrhagic Fever (CCHF) infection by utilizing the CRISPR/Cas13b system. CCHF, an RNA virus, poses a significant public health threat to our country due to its high mortality rate and the lack of effective therapeutic measures. The CRISPR/Cas13b system, known for its RNA-targeting capabilities, was chosen for its potential to degrade viral RNA and inhibit viral replication.

Studies focusing on CRISPR/Cas13-based viral RNA knockdown have demonstrated its potent ability to specifically target and degrade viral RNA within infected cells. These investigations have shown Cas13's potential against a range of RNA viruses, including influenza, Zika, and SARS-CoV-2. By designing guide RNAs complementary to essential viral RNA sequences, significant reductions in viral replication and load was observed. As an example, in studies on SARS-CoV-2, Cas13 effectively cleaved viral RNA, inhibiting the virus's ability to replicate and spread. This work has also highlighted the enzyme's high specificity, reducing the risk of off-target effects on host cellular RNA. However, challenges such as the efficient delivery of the Cas13 system into host cells and potential immune responses remain to be addressed. In our study, we successfully demonstrated that Cas13 cleaves viral RNA *in vitro*. We targeted and cleaved the CCHF virus RNA, which had not been done before, making our study unique. To combat the challenge of efficient delivery, we utilized AAV systems because AAV vectors have high transduction efficiency, minimal cytotoxic effects, low immunogenicity, and can provide long-term gene expression without incorporating into the host genome.

Our approach involved several vital steps. After determining the optimum conditions, we cloned the Cas13b enzyme into a plasmid and induced Cas13b expression in E. coli. The Cas13b protein was subsequently purified using Fast Protein Liquid Chromatography (FPLC). Guide RNAs (gRNAs) were designed to target the viral S genome segment, which encodes the nucleocapsid protein essential for viral replication. The *in silico* design of gRNAs was performed using CRISPR-RT, EMBOSS Needle, and RNAfold tools to ensure specificity and efficacy.

The viral genome material, provided by our collaborators at Ankara University in a plasmid, was transcribed into RNA through *In vitro* Transcription (IVT). Similarly, gRNAs were also synthesized via IVT. An *in vitro* cleavage assay was designed to test the efficacy of the CRISPR/Cas13b system. The assay components included Cas13b, gRNA, and the target RNA. Through optimization of the reaction conditions, we successfully demonstrated the *in vitro* activity of Cas13b in degrading the target viral RNA.

In the second part of the project, we focused on the delivery of CRISPR/Cas13b agents to mammalian cells. HEK293 cells were chosen for this purpose, and adeno-associated virus (AAV) was used as the gene delivery agent. AAV vectors were selected due to their high transduction efficiency, minimal cytogenic effects, low immunogenicity, and ability to provide long-term gene expression without incorporating into the host genome. Cas13b, gRNA, and the direct repeat (DR) region were cloned into an AAV expression vector. The AAV vector was then co-transfected with helper plasmid and DJ plasmid into HEK293 cells to induce viral particle creation. The successful delivery of the CRISPR/Cas13b system was confirmed by a PCR reaction for Cas13b gene amplification. This indicated that the HEK293 cells expressed the vector plasmid

carrying the CRISPR/Cas13b agents, including the Cas13b gene and the corresponding gRNA.

The results of this study provide a promising foundation for developing CRISPR/Cas13b-based antiviral therapies. The successful *in vitro* demonstration of Cas13b activity against the CCHF viral RNA, coupled with effective delivery to mammalian cells, underscores the potential of this approach to inhibit viral replication and combat the infection.

This study contributes to the broader field of antiviral therapy by highlighting the effectiveness of RNA-targeted gene editing tools. The insights gained from this research could lead to developing specific and safe therapeutic strategies for CCHF and other RNA viruses. Future work will focus on optimizing delivery systems for in vivo applications and evaluating the long-term efficacy and safety of this approach in clinical settings. Our research has shown that the CRISPR/Cas13b system can effectively target and degrade CCHF viral RNA. This innovative approach represents a significant step forward in the fight against CCHF and holds promise for addressing other RNA viral infections through similar methodologies.

BIBLIORGRAPHY

[1] J.P. Messina, D.M. Pigott, N. Golding, K.A. Duda, J.S. Brownstein, D.J. Weiss, H. Gibson, T.P. Robinson, M. Gilbert, G.R. William Wint, P.A. Nuttall, P.W. Gething, M.F. Myers, D.B. George, S.I. Hay, The global distribution of Crimean-Congo hemorrhagic fever, Trans. R. Soc. Trop. Med. Hyg. 109 (2015) 503–513. https://doi.org/10.1093/trstmh/trv050.

[2] B. Wahid, S. Altaf, N. Naeem, N. Ilyas, M. Idrees, Scoping Review of Crimean-Congo Hemorrhagic Fever (CCHF) Literature and Implications of Future Research, J. Coll. Physicians Surg.--Pak. JCPSP 29 (2019) 563–573. https://doi.org/10.29271/jcpsp.2019.06.563.

[3] H. Hoogstraal, The epidemiology of tick-borne Crimean-Congo hemorrhagic fever in Asia, Europe, and Africa, J. Med. Entomol. 15 (1979) 307–417. https://doi.org/10.1093/jmedent/15.4.307.

[4] T. Tipih, F.J. Burt, Crimean-Congo Hemorrhagic Fever Virus: Advances in Vaccine Development, BioResearch Open Access 9 (2020) 137–150. https://doi.org/10.1089/biores.2019.0057.

[5] C.A. Whitehouse, Crimean-Congo hemorrhagic fever, Antiviral Res. 64 (2004) 145–160. https://doi.org/10.1016/j.antiviral.2004.08.001.

[6] D.A. Bente, N.L. Forrester, D.M. Watts, A.J. McAuley, C.A. Whitehouse, M. Bray, Crimean-Congo hemorrhagic fever: History, epidemiology, pathogenesis, clinical syndrome and genetic diversity, Antiviral Res. 100 (2013) 159–189. https://doi.org/10.1016/j.antiviral.2013.07.006.

[7] O. Ergönül, A. Celikbaş, B. Dokuzoguz, S. Eren, N. Baykam, H. Esener, Characteristics of patients with Crimean-Congo hemorrhagic fever in a recent

outbreak in Turkey and impact of oral ribavirin therapy, Clin. Infect. Dis. Off. Publ. Infect. Dis. Soc. Am. 39 (2004) 284–287. https://doi.org/10.1086/422000.

[8] F. Duygu, A.C. Cicek, T. Kaya, Crimean-Congo hemorrhagic fever and pregnancy: Two cases, J. Microbiol. Infect. Dis. 5 (2015) 29–31. https://doi.org/10.5799/ahinjs.02.2015.01.0171.

[9] S.P. Fabara, J.F. Ortiz, D.W. Smith, J. Parwani, S. Srikanth, T. Varghese, M. Paez, P. Desai, R. Tirupathi, Crimean-Congo Hemorrhagic Fever Beyond Ribavirin: A Systematic Review, Cureus 13 (2021) e17842. https://doi.org/10.7759/cureus.17842.

[10] Ö. Ergönül, Crimean-Congo haemorrhagic fever, Lancet Infect. Dis. 6 (2006) 203–214. https://doi.org/10.1016/S1473-3099(06)70435-2.

[11] G.R. Yilmaz, T. Buzgan, H. Irmak, A. Safran, R. Uzun, M.A. Cevik, M.A. Torunoglu, The epidemiology of Crimean-Congo hemorrhagic fever in Turkey, 2002-2007, Int. J. Infect. Dis. IJID Off. Publ. Int. Soc. Infect. Dis. 13 (2009) 380–386. https://doi.org/10.1016/j.ijid.2008.07.021.

[12] H. Leblebicioglu, R. Ozaras, H. Irmak, I. Sencan, Crimean-Congo hemorrhagic fever in Turkey: Current status and future challenges, Antiviral Res. 126 (2016) 21–34. https://doi.org/10.1016/j.antiviral.2015.12.003.

[13] Z. Vatansever, R.U. DVM, A. Estrada-Pena, O. Ergonul, Crimean-Congo Hemorrhagic Fever in Turkey, in: O. Ergonul, C.A. Whitehouse (Eds.), Crime.-Congo Hemorrhagic Fever Glob. Perspect., Springer Netherlands, Dordrecht, 2007: pp. 59–74. https://doi.org/10.1007/978-1-4020-6106-6_6.

[14] K. Ergünay, C. Polat, A. Özkul, Vector-borne viruses in Turkey: A systematic review and bibliography, Antiviral Res. 183 (2020) 104934. https://doi.org/10.1016/j.antiviral.2020.104934.

[15] C. Leyrat, F. Yabukarski, N. Tarbouriech, E.A.R. Jr, M.R. Jensen, M. Blackledge, R.W.H. Ruigrok, M. Jamin, Structure of the Vesicular Stomatitis Virus N0-P Complex, PLOS Pathog. 7 (2011) e1002248. https://doi.org/10.1371/journal.ppat.1002248.

[16] I. Andersson, M. Simon, A. Lundkvist, M. Nilsson, A. Holmström, F. Elgh, A. Mirazimi, Role of actin filaments in targeting of Crimean Congo hemorrhagic fever virus nucleocapsid protein to perinuclear regions of mammalian cells, J. Med. Virol. 72 (2004) 83–93. https://doi.org/10.1002/jmv.10560.

[17] Y. Wang, S. Dutta, H. Karlberg, S. Devignot, F. Weber, Q. Hao, Y.J. Tan, A. Mirazimi, M. Kotaka, Structure of Crimean-Congo hemorrhagic fever virus nucleoprotein: superhelical homo-oligomers and the role of caspase-3 cleavage, J. Virol. 86 (2012) 12294–12303. https://doi.org/10.1128/JVI.01627-12.

[18] A. Moming, D. Tuoken, X. Yue, W. Xu, R. Guo, D. Liu, Y. Li, Z. Hu, F. Deng, Y. Zhang, S. Sun, Mapping of B-cell epitopes on the N- terminal and C-terminal segment of nucleocapsid protein from Crimean-Congo hemorrhagic fever virus, PLoS ONE 13 (2018) e0204264. https://doi.org/10.1371/journal.pone.0204264.

[19] H.A. Bendary, F. Rasslan, M. Wainwright, S. Alfarraj, A.M. Zaki, A.K. Abdulall, Crimean-Congo hemorrhagic fever virus in ticks collected from imported camels in Egypt, Saudi J. Biol. Sci. 29 (2022) 2597–2603. https://doi.org/10.1016/j.sjbs.2021.12.043.

[20] A. Portillo, A.M. Palomar, P. Santibáñez, J.A. Oteo, Epidemiological Aspects of Crimean-Congo Hemorrhagic Fever in Western Europe: What about the Future?, Microorganisms 9 (2021) 649. https://doi.org/10.3390/microorganisms9030649.

[21] M. Simon, C. Johansson, A. Mirazimi, Crimean-Congo hemorrhagic fever virus entry and replication is clathrin-, pH- and cholesterol-dependent, J. Gen. Virol. 90 (2009) 210–215. https://doi.org/10.1099/vir.0.006387-0.

[22] X. Xiao, Y. Feng, Z. Zhu, D.S. Dimitrov, Identification of a putative Crimean-Congo hemorrhagic fever virus entry factor, Biochem. Biophys. Res. Commun. 411 (2011) 253–258. https://doi.org/10.1016/j.bbrc.2011.06.109.

[23] D.P. Clark, N.J. Pazdernik, M.R. McGehee, Chapter 24 - Viruses, Viroids, and Prions, in: D.P. Clark, N.J. Pazdernik, M.R. McGehee (Eds.), Mol. Biol. Third Ed., Academic Cell, 2019: pp. 749–792. https://doi.org/10.1016/B978-0-12-813288-3.00024-0.

[24] J.H. STRAUSS, E.G. STRAUSS, Minus-Strand RNA Viruses, Viruses Hum. Dis. (2008) 137–191. https://doi.org/10.1016/B978-0-12-373741-0.50007-6.

[25] Kırım Kongo Kanamalı Ateşi, (n.d.). https://hsgm.saglik.gov.tr/tr/zoonotik-ve-vektorel-hastaliklar/kkka.html (accessed May 20, 2024).

[26] A.C.R. Hoste, I. Djadjovski, M.Á. Jiménez-Clavero, P. Rueda, J.N. Barr, P. Sastre, Multiplex Assay for Simultaneous Detection of Antibodies against Crimean-Congo Hemorrhagic Fever Virus Nucleocapsid Protein and Glycoproteins in Ruminants, Microbiol. Spectr. 11 (2023) e0260022. https://doi.org/10.1128/spectrum.02600-22.

[27] A. Ahmed, Y. Ali, B. Salim, I. Dietrich, J. Zinsstag, Epidemics of Crimean-Congo Hemorrhagic Fever (CCHF) in Sudan between 2010 and 2020, Microorganisms 10 (2022) 928. https://doi.org/10.3390/microorganisms10050928.

[28] Y. Ishino, H. Shinagawa, K. Makino, M. Amemura, A. Nakata, Nucleotide sequence of the iap gene, responsible for alkaline phosphatase isozyme

conversion in Escherichia coli, and identification of the gene product, J. Bacteriol. 169 (1987) 5429–5433. https://doi.org/10.1128/jb.169.12.5429-5433.1987.

[29] F.J. Mojica, G. Juez, F. Rodríguez-Valera, Transcription at different salinities of Haloferax mediterranei sequences adjacent to partially modified PstI sites, Mol. Microbiol. 9 (1993) 613–621. https://doi.org/10.1111/j.1365-2958.1993.tb01721.x.

[30] F.J.M. Mojica, C. Díez-Villaseñor, J. García-Martínez, E. Soria, Intervening sequences of regularly spaced prokaryotic repeats derive from foreign genetic elements, J. Mol. Evol. 60 (2005) 174–182. https://doi.org/10.1007/s00239-004-0046-3.

[31] R. Jansen, J.D.A. van Embden, W. Gaastra, L.M. Schouls, Identification of genes that are associated with DNA repeats in prokaryotes, Mol. Microbiol. 43 (2002) 1565–1575. https://doi.org/10.1046/j.1365-2958.2002.02839.x.

[32] K.S. Makarova, N.V. Grishin, S.A. Shabalina, Y.I. Wolf, E.V. Koonin, A putative RNA-interference-based immune system in prokaryotes: computational analysis of the predicted enzymatic machinery, functional analogies with eukaryotic RNAi, and hypothetical mechanisms of action, Biol. Direct 1 (2006) 7. https://doi.org/10.1186/1745-6150-1-7.

[33] E.V. Koonin, K.S. Makarova, Origins and evolution of CRISPR-Cas systems, Philos. Trans. R. Soc. Lond. B. Biol. Sci. 374 (2019) 20180087. https://doi.org/10.1098/rstb.2018.0087.

[34] J.A. Doudna, E. Charpentier, The new frontier of genome engineering with CRISPR-Cas9, Science 346 (2014) 1258096. https://doi.org/10.1126/science.1258096.

[35] A.A. Smargon, D.B.T. Cox, N.K. Pyzocha, K. Zheng, I.M. Slaymaker, J.S. Gootenberg, O.A. Abudayyeh, P. Essletzbichler, S. Shmakov, K.S. Makarova, E.V. Koonin, F. Zhang, Cas13b is a Type VI-B CRISPR-associated RNA-Guided RNAse differentially regulated by accessory proteins Csx27 and Csx28, Mol. Cell 65 (2017) 618. https://doi.org/10.1016/j.molcel.2016.12.023.

[36] J. Gao, T. Luo, N. Lin, S. Zhang, J. Wang, A New Tool for CRISPR-Cas13a-Based Cancer Gene Therapy, Mol. Ther. Oncolytics 19 (2020) 79–92. https://doi.org/10.1016/j.omto.2020.09.004.

[37] S. Shmakov, A. Smargon, D. Scott, D. Cox, N. Pyzocha, W. Yan, O.O. Abudayyeh, J.S. Gootenberg, K.S. Makarova, Y.I. Wolf, K. Severinov, F. Zhang, E.V. Koonin, Diversity and evolution of class 2 CRISPR–Cas systems, Nat. Rev. Microbiol. 15 (2017) 169–182. https://doi.org/10.1038/nrmicro.2016.184.

[38] Y. Xue, Z. Chen, W. Zhang, J. Zhang, Engineering CRISPR/Cas13 System against RNA Viruses: From Diagnostics to Therapeutics, Bioengineering 9 (2022) 291. https://doi.org/10.3390/bioengineering9070291.

[39] Y. Tang, Y. Fu, Class 2 CRISPR/Cas: an expanding biotechnology toolbox for and beyond genome editing, Cell Biosci. 8 (2018) 59. https://doi.org/10.1186/s13578-018-0255-x.

[40] J.S. Gootenberg, O.O. Abudayyeh, J.W. Lee, P. Essletzbichler, A.J. Dy, J. Joung, V. Verdine, N. Donghia, N.M. Daringer, C.A. Freije, C. Myhrvold, R.P. Bhattacharyya, J. Livny, A. Regev, E.V. Koonin, D.T. Hung, P.C. Sabeti, J.J. Collins, F. Zhang, Nucleic acid detection with CRISPR-Cas13a/C2c2, Science 356 (2017) 438–442. https://doi.org/10.1126/science.aam9321.

[41] N. Huynh, N. Depner, R. Larson, K. King-Jones, A versatile toolkit for CRISPR-Cas13-based RNA manipulation in Drosophila, Genome Biol. 21 (2020) 279. https://doi.org/10.1186/s13059-020-02193-y.

[42] C.M. Ackerman, C. Myhrvold, S.G. Thakku, C.A. Freije, H.C. Metsky, D.K. Yang, S.H. Ye, C.K. Boehm, T.-S.F. Kosoko-Thoroddsen, J. Kehe, T.G. Nguyen, A. Carter, A. Kulesa, J.R. Barnes, V.G. Dugan, D.T. Hung, P.C. Blainey, P.C. Sabeti, Massively multiplexed nucleic acid detection with Cas13, Nature 582 (2020) 277–282. https://doi.org/10.1038/s41586-020-2279-8.

[43] D.B.T. Cox, J.S. Gootenberg, O.O. Abudayyeh, B. Franklin, M.J. Kellner, J. Joung, F. Zhang, RNA editing with CRISPR-Cas13, Science 358 (2017) 1019–1027. https://doi.org/10.1126/science.aaq0180.

[44] S. Konermann, P. Lotfy, N.J. Brideau, J. Oki, M.N. Shokhirev, P.D. Hsu, Transcriptome Engineering with RNA-Targeting Type VI-D CRISPR Effectors, Cell 173 (2018) 665-676.e14. https://doi.org/10.1016/j.cell.2018.02.033.

[45] S.S. Bawage, P.M. Tiwari, P.J. Santangelo, Synthetic mRNA expressed Cas13a mitigates RNA virus infections, (2018) 370460. https://doi.org/10.1101/370460.

[46] M. Kordyś, R. Sen, Z. Warkocki, Applications of the versatile CRISPR-Cas13 RNA targeting system, WIREs RNA 13 (2022) e1694. https://doi.org/10.1002/wrna.1694.

[47] V.E. Hillary, S.A. Ceasar, A Review on the Mechanism and Applications of CRISPR/Cas9/Cas12/Cas13/Cas14 Proteins Utilized for Genome Engineering, Mol. Biotechnol. 65 (2023) 311–325. https://doi.org/10.1007/s12033-022-00567-0.

[48] O.O. Abudayyeh, J.S. Gootenberg, P. Essletzbichler, S. Han, J. Joung, J.J. Belanto, V. Verdine, D.B.T. Cox, M.J. Kellner, A. Regev, E.S. Lander, D.F.

Voytas, A.Y. Ting, F. Zhang, RNA targeting with CRISPR–Cas13, Nature 550 (2017) 280–284. https://doi.org/10.1038/nature24049.

[49] Z. Zhang, J. Chen, Z. Zhu, Z. Zhu, X. Liao, J. Wu, J. Cheng, X. Zhang, H. Mei, G. Yang, CRISPR-Cas13-Mediated Knockdown of lncRNA-GACAT3 Inhibited Cell Proliferation and Motility, and Induced Apoptosis by Increasing p21, Bax, and E-Cadherin Expression in Bladder Cancer, Front. Mol. Biosci. 7 (2021). https://doi.org/10.3389/fmolb.2020.627774.

[50] N. Zhang, B. Bewick, G. Xia, D. Furling, T. Ashizawa, A CRISPR-Cas13a Based Strategy That Tracks and Degrades Toxic RNA in Myotonic Dystrophy Type 1, Front. Genet. 11 (2020) 594576. https://doi.org/10.3389/fgene.2020.594576.

[51] G. Kushawah, L. Hernandez-Huertas, J. Abugattas-Nuñez Del Prado, J.R. Martinez-Morales, M.L. DeVore, H. Hassan, I. Moreno-Sanchez, L. Tomas-Gallardo, A. Diaz-Moscoso, D.E. Monges, J.R. Guelfo, W.C. Theune, E.O. Brannan, W. Wang, T.J. Corbin, A.M. Moran, A. Sánchez Alvarado, E. Málaga-Trillo, C.M. Takacs, A.A. Bazzini, M.A. Moreno-Mateos, CRISPR-Cas13d Induces Efficient mRNA Knockdown in Animal Embryos, Dev. Cell 54 (2020) 805-817.e7. https://doi.org/10.1016/j.devcel.2020.07.013.

[52] B. He, W. Peng, J. Huang, H. Zhang, Y. Zhou, X. Yang, J. Liu, Z. Li, C. Xu, M. Xue, H. Yang, P. Huang, Modulation of metabolic functions through Cas13d-mediated gene knockdown in liver, Protein Cell 11 (2020) 518–524. https://doi.org/10.1007/s13238-020-00700-2.

[53] E.L. Blanchard, D. Vanover, S.S. Bawage, P.M. Tiwari, L. Rotolo, J. Beyersdorf, H.E. Peck, N.C. Bruno, R. Hincapie, F. Michel, J. Murray, H. Sadhwani, B. Vanderheyden, M.G. Finn, M.A. Brinton, E.R. Lafontaine, R.J.

Hogan, C. Zurla, P.J. Santangelo, Treatment of influenza and SARS-CoV-2 infections via mRNA-encoded Cas13a in rodents, Nat. Biotechnol. 39 (2021) 717–726. https://doi.org/10.1038/s41587-021-00822-w.

[54] L. Yin, F. Zhao, H. Sun, Z. Wang, Y. Huang, W. Zhu, F. Xu, S. Mei, X. Liu, D. Zhang, L. Wei, S. Cen, S. Hu, C. Liang, F. Guo, CRISPR-Cas13a Inhibits HIV-1 Infection, Mol. Ther. Nucleic Acids 21 (2020) 147–155. https://doi.org/10.1016/j.omtn.2020.05.030.

[55] M.U. Ashraf, H.M. Salman, M.F. Khalid, M.H.F. Khan, S. Anwar, S. Afzal, M. Idrees, S.U. Chaudhary, CRISPR-Cas13a mediated targeting of hepatitis C virus internal-ribosomal entry site (IRES) as an effective antiviral strategy, Biomed. Pharmacother. 136 (2021) 111239. https://doi.org/10.1016/j.biopha.2021.111239.

[56] R. Aman, A. Mahas, H. Butt, Z. Ali, F. Aljedaani, M. Mahfouz, Engineering RNA Virus Interference via the CRISPR/Cas13 Machinery in Arabidopsis, Viruses 10 (2018) 732. https://doi.org/10.3390/v10120732.

[57] C. Li, L. Guo, G. Liu, M. Guo, H. Wei, Q. Yang, J. Wang, H. Chen, Reprogrammed CRISPR-Cas13a targeting the HPV16/18 E6 gene inhibits proliferation and induces apoptosis in E6-transformed keratinocytes, Exp. Ther. Med. 19 (2020) 3856–3860. https://doi.org/10.3892/etm.2020.8631.

[58] H. Li, S. Wang, X. Dong, Q. Li, M. Li, J. Li, Y. Guo, X. Jin, Y. Zhou, H. Song, Z. Kou, CRISPR-Cas13a Cleavage of Dengue Virus NS3 Gene Efficiently Inhibits Viral Replication, Mol. Ther. Nucleic Acids 19 (2020) 1460–1469. https://doi.org/10.1016/j.omtn.2020.01.028.

[59] T.R. Abbott, G. Dhamdhere, Y. Liu, X. Lin, L. Goudy, L. Zeng, A. Chemparathy, S. Chmura, N.S. Heaton, R. Debs, T. Pande, D. Endy, M.F. La

Russa, D.B. Lewis, L.S. Qi, Development of CRISPR as an Antiviral Strategy to Combat SARS-CoV-2 and Influenza, Cell 181 (2020) 865-876.e12. https://doi.org/10.1016/j.cell.2020.04.020.

[60] M. Adachi, M. Fukuda, E. Nishida, Nuclear Export of Map Kinase (ERK) Involves a Map Kinase Kinase (Mek-Dependent) Active Transport Mechanism, J. Cell Biol. 148 (2000) 849–856.

[61] J.A. Bornhorst, J.J. Falke, [16] Purification of Proteins Using Polyhistidine Affinity Tags, Methods Enzymol. 326 (2000) 245–254.

[62] M. Fathi-Roudsari, A. Akhavian-Tehrani, N. Maghsoudi, Comparison of Three Escherichia coli Strains in Recombinant Production of Reteplase, Avicenna J. Med. Biotechnol. 8 (2016) 16.

[63] R. Gl, C. Ea, Recombinant protein expression in Escherichia coli: advances and challenges, Front. Microbiol. 5 (2014). https://doi.org/10.3389/fmicb.2014.00172.

[64] R.J. Sundberg, R.B. Martin, Interactions of histidine and other imidazole derivatives with transition metal ions in chemical and biological systems, Chem. Rev. 74 (1974) 471–517. https://doi.org/10.1021/cr60290a003.

[65] J. Crowe, B.S. Masone, J. Ribbe, One-Step Purification of Recombinant Proteins with the 6xHis Tag and Ni-NTA Resin, in: A.J. Harwood (Ed.), Basic DNA RNA Protoc., Humana Press, Totowa, NJ, 1996: pp. 491–510. https://doi.org/10.1385/0-89603-402-X:491.

[66] B. Zetsche, J.S. Gootenberg, O.O. Abudayyeh, I.M. Slaymaker, K.S. Makarova, P. Essletzbichler, S.E. Volz, J. Joung, J. van der Oost, A. Regev, E.V. Koonin, F. Zhang, Cpf1 is a single RNA-guided endonuclease of a class 2 CRISPR-Cas system, Cell 163 (2015) 759–771. https://doi.org/10.1016/j.cell.2015.09.038.

[67] M.T. Reetz, M.H. Becker, H.-W. Klein, D. Stöckigt, A Method for High-Throughput Screening of Enantioselective Catalysts, Angew. Chem. Int. Ed Engl. 38 (1999) 1758–1761. https://doi.org/10.1002/(SICI)1521-3773(19990614)38:12<1758::AID-ANIE1758>3.0.CO;2-8.

[68] I. Chen, B.M. Dorr, D.R. Liu, A general strategy for the evolution of bond-forming enzymes using yeast display, Proc. Natl. Acad. Sci. 108 (2011) 11399–11404. https://doi.org/10.1073/pnas.1101046108.

[69] N.E. Good, G.D. Winget, W. Winter, T.N. Connolly, S. Izawa, R.M.M. Singh, Hydrogen Ion Buffers for Biological Research*, Biochemistry 5 (1966) 467–477. https://doi.org/10.1021/bi00866a011.

[70] C. Mateo, J.M. Palomo, G. Fernandez-Lorente, J.M. Guisan, R. Fernandez-Lafuente, Improvement of enzyme activity, stability and selectivity via immobilization techniques, Enzyme Microb. Technol. 40 (2007) 1451–1463. https://doi.org/10.1016/j.enzmictec.2007.01.018.

[71] M. Kanai, K. Hikino, S. Mano, Cloning and Functional Verification of Endogenous U6 Promoters for the Establishment of Efficient CRISPR/Cas9-Based Genome Editing in Castor (Ricinus communis), Genes 14 (2023) 1327. https://doi.org/10.3390/genes14071327.

[72] P. Luo, S. Li, L. Li, Y. Li, Y. Qiao, X. Wu, M. Wu, Z. Song, Y. Yang, J. Feng, X. Tang, Validation of endogenous U6 promoters for expanding the CRISPR toolbox in Nicotiana tabacum, Vitro Cell. Dev. Biol. - Plant 60 (2024) 378–383. https://doi.org/10.1007/s11627-024-10418-z.

[73] D. Grimm, A. Kern, K. Rittner, J.A. Kleinschmidt, Novel tools for production and purification of recombinant adenoassociated virus vectors, Hum. Gene Ther. 9 (1998) 2745–2760. https://doi.org/10.1089/hum.1998.9.18-2745.

[74] J.E. Rabinowitz, J. Samulski, Adeno-associated virus expression systems for gene transfer, Curr. Opin. Biotechnol. 9 (1998) 470–475. https://doi.org/10.1016/s0958-1669(98)80031-1.

[75] D. Grimm, J.S. Lee, L. Wang, T. Desai, B. Akache, T.A. Storm, M.A. Kay, In Vitro and In Vivo Gene Therapy Vector Evolution via Multispecies Interbreeding and Retargeting of Adeno-Associated Viruses, J. Virol. 82 (2008) 5887–5911. https://doi.org/10.1128/JVI.00254-08.

[76] F.L. Graham, J. Smiley, W.C. Russell, R. Nairn, Characteristics of a Human Cell Line Transformed by DNA from Human Adenovirus Type 5, J. Gen. Virol. 36 (1977) 59–72. https://doi.org/10.1099/0022-1317-36-1-59.

APPENDIX A

DNA SEQUENCES OF CONSTRUCTS

Table A. 1: Gene sequences and regulatory elements used in this study

Gene Name	**Sequence**
RanCas13b	GATCTGGGACTTCACGATCTCACAGTACTCCCTCAGCAC CTTCAGCAGGGCCTCTGCGATTCCCAGGCCATCCTTCTCC TCTGTGGTGGGCTGGGCCACGGTGAACAGTGGGATAGGG GCGTGCAGGGCCTCCTTGTAGAAGGGGTACTGGTTGTGG CAGAAGGCATTGCGCACGCTGGCGATGAAGGCGATGTG CTCGTCTGTCACCATGGAGCTGGCGGCATACTCCTTCTTC CACTCCTCCAGCAGGGCCCTAAACTCGTTCTCCAGAGAG GACAGGGATGTGTGCTTATTCAGCAGCTTCTCCTCCAGG CTCAGTGTCTCCTTGAAGGCGTCCACTCTCAGAGACTGG TAGATCTCCAGCTCGCGCCTCAGCCGCAGCTGGCTGATT GGGTGCTTCTGTGTATCGTTCTCCTCCTTGATAAAAGAGA ACAGGCCATTCAGTCTCCGGTCCTTCACCAGGGCCTTGA AGTTGCCCATCTTCAGGGCCTTGGTGTGCTCCTCGCGGAT ATACACTGTCCTGATTGGGGTCTTGTGGTACTGCACCTCG CCAAAGGCTGTGGCAGGGTACACCTTCACAGGCAGCACC ATGGGCAGGGTCTGATTCAGAGGGTTCAGCTTGGCATCG GCCTCCTGCACGTTCACGGCCAGATTCTCCAGCTTCAGCT GGTGATAATTCAGGTTCAGCTCCTTGAAGTGGTTCTTTGT CAGCTCCAGGGTCATCAGCCACAGCATCACGTCCTGATT CCGGTACAGCCGCAGCTTCTTCTCCAGGTGCTGCCATCTC TTATACAGCAGGTAATCCTTCCAGCGGTCGCTTGTGTGC AGCTCCAGCCTCTGGCTCTCGGTTGGAGACTGAGGCTTG TTCTGCTGCCAATACTCGTAGTGCTCCTCCCGCTTCAGCA GTGGTGCCTTTGCCTCCAGCTTATAGGACAGATTGTAGA AGCTCTGGTGCTTATCCTGATACTTCTCCTTAAAGTACAG GGTGATGGCTCTGCTGATGAAGCCCACCCGGCCGTGCTT CTTGATCTCCTTGCGGATTGGCTTGCTCAGCATCAGGTCC TCAGACAGTGTCTCTCTGATGGCCTCGGTAAACAGGCCC CGTGGCAGAGAGATTCCTCCCTGCTCCCATCCCTTCACCA GATTCTTCCTGTTCTCCTTAGGGATCTTCAGCAGCAGGCA ATACTGGTAGGGCTCCCATGGCTGGTTCTTGATGGCCTCC AGAAACTTCTCGCGCTGCTCCAGATACTGCTGGTAGAAA TCCACCAGATTCCTGCAGGCCTTCCAATTAAACTTGTTCA GGAAGGGGTGTGGATTTGTGTTGCCGATCAGGTTGGTCT GCTTGAAATAGCCCTCCAGCCTATTCTTCTCTCCTCCGTA CAGGGCCAGGGCGCGCCTGATAAACCAGAACTCGGTGG AGTTGGCCTTGCTAGACTTGATAGGCTGATTCTGGGCGT CGTAGGCCACGGGCTGAAAGCGCATGAAATCCTTCACCA GCCAGTCGGCCAGCACGCCTGTCTTGATCAGCTTCTCTCT

	CCGCTTGCCCAGCTTTGGGGAGCTCTTCAGCTTTGTGTTC AGCCTGTGAGACAGCAGCTTTGTCTCGGCGATCAGCTTC TCGATCTTGATCTTGGCCTTCTCGGACAGATCAGGCTGCT TATTCTGCAGCAGGCCCAGCATCTGCTTGGGAAAGGCTC CCAGTGGCAGTCTGCCCTGGTTTGCCTTCTCCAGATCCTC GATGGTATTGATCCGCTCCTCCTCGAAGTCCTTATAGATT CTCTGGATGTGCCGCACTGTCTCCTTCAGCAGGTCCTCGC TCTTGCCGGTCAGGTGCTGGTAGAACATCAGAGGCAGCA GCTCGTGCACAGAGATAAAGGCGTGGGCCACGAAGCCG GAGTTATAAGGGTACTTGGCGATTCTATTGGCGCCATCC TTGATCTCCAGGGAGGGGTACAGCTCCTTGCTTGTGCCC AGCCGAAAGCCGATCTTGTTGTCGGTGATGTGATAGTGT GGTGTGGTCTTAGAGATGAAAGGCTGATTGGATGTCTCC TTGTAATCCAGGTCCTTGGTCAGGGCCTTCCACTCCTGGG GTCTGTTGATCTCGGTAAAGTCCTGCAGCCGGCCGAAGG ACAGCAGTGTGCGGGTCAGGTGCCTCTTCTCCTGCTCATC GCCGATCTTCTTGTCGTAGATACAATAGTGGTATGTGCCC AGATCCACCTGAAAGCGGATAGACTTGAAGGACTCATTC AGGTCCAGATACCTCAGGGCAAAGTAGGGGAATCTATCC TGGTGCCGGATCAGGGTGTCCTTGAATGGGTTCTGCTCCT CCTCGATCTCATCCAGAAAGCCGTCGGCCTCCACCTGGA AGTGCTTCTTATTCTCCTCGCTCAGCTTCTCATACAGCAG CTTAGGACATCTGCTCAGCTCAGACAGCATATCCAGCAG CATCTGGTTGTGGTCGTAGCGGGACTCCAGCCTCAGCTT GGGCAGCAGGATGCGGCTCCTGCAAAACACCTCTGTGGT CATCTTCTCGCGCTGCTTGTGAGAGGCCTTGAAGCCGGA CACCTTCTTCAGCATCCAATAGGCATCCCTCTTGTCCAGA AACAGATTTGTAAAGAACAGCAGGCCAGACTCGGTAAA GAAGCCATCCTTCTCGAATCTGTATCTGTTGAAGTCGGG ATTGTCCTGCTTGTTCTTGCCCTTGCGGTTCAGGTGGGCA AAGTCCCTTGTCAGATTCACGGTGAAGTGGGCCTTATAA TCCTCCTTCACCATTCTCAGAGAGGCGTCGAAGGCCTTAT ACAGGTGCTTGAAGATATCCTTCTCGGCGTCGGGCTTCTT GTGCTTATAGTGGCTATAGTAGTTCCGCAGAGAGTGCAG CTGATTCACCAGGATCTCCAGGGCCTCGATCAGCTTGGA TGGGTTCAGGGCCTCTGCCTGGGACTGTGCCTCGCTCTCC TTCTCCTTCTGCTGCTCCTTCTGGTGGCCCTTCTTCTTGCC CTCCTTCTTAGGGGGGTGGTAGCACATGGCTGTCAGAAA AGGGAAGTGCTTCAGGATCAGCTCGGTCAGCTGGGACTT CTTCAGCAGATCGTGGTCATTGTTCAGGATATTGTTCCAT GTCTCGCACACCACGTCCACGATCTTATCGTCGTTGCTGG GGGTTTTCAGGCCCAGCTGCTCATTGATGTGGCAGATGG TGATAAAGGCGTTGTGCCGGGCGATATTCAGGAAGGCGC CCCAAAAGAACTTGTGCTTCAGGGTATACACGTTAGGCA GCAGGGGCTTCTCCAT
MapK NES	AGCCTCCAAAAAAAGTTGGAGGAATTAGAACTA
Kozak Sequence	GCCACC

T7 promoter	TAATACGACTCACTATAG
T7 terminator	TAGCATAACCCCTTGGGGCCTCTAAACGGGTCTTGAGGGGTTTTTTG
gRNA S1	TTTATAAAAATTCATCTGCTCTTCGTGCA
gRNA L1	CAGCTAGATACAGGGCAGCTGTTATTGGT
Direct repeat (DR)	GTTGGGACTGCTCTCACTTTGAAGGGTATTCACAAC
U6 promoter	GAGGGCCTATTTCCCATGATTCCTTCATATTTGCATATACGATACAAGGCTGTTAGAGAGATAATTAGAATTAATTTGACTGTAAACACAAAGATATTAGTACAAAATACGTGACGTAGAAAGTAATAATTTCTTGGGTAGTTTGCAGTTTTAAAATTATGTTTTAAAATGGACTATCATATGCTTACCGTAACTTGAAAGTATTTCGATTTCTTGGCTTTATATATCTTGTGGAAAGGAC
U6 terminator	TTTTTTT
His-tag	CACCACCACCACCACCAC

APPENDIX B

LIST OF PRIMERS

Table B. 1: Primer sequences used for cloning of constructs

Primer Name	Sequence (5'-3')
EA1	CTCTAGATTAACTTTAAGAAGGAGGGTACCGCCACCATGGAGAAGCCCCT
EA2	ATCTCAGTGGTGGTGGTGGTGGTGCTCGAGTAGTTCTAATTCCTCCAACTTTTTTTGGAGGCTGG
EA3	AGTCCCAACTTTGCACGAAGAGCAGATGAATTTTTATAAACCCTATAGTGAGTCGTATTAGAATTATTTC
EA4	GCTCTCACTTTGAAGGGTATTCACAACTAGCATAACCCCTTGGGGCCTCTAAACGGGTCTTGAGGGGTTTTTTG
EA5	GGCAAAGAATTGGGATTCGAACATCGATTGAATTCGCCACCATGGAGAAGCCCCTG
EA6	GAGGCAAGCTTCTGCAGGTCGACTCTAGAG GATCCTCAGTGGTGGTGGTGGTGGTGCTC
EA7	GGCCAACTCCATCACTAGGGGTTCCTGCGGCCGCAGGTA CCGAGGGCCTATTTCCCATG
EA8	GTTGTGAATACCCTTCAAAGTGAGAGCAGTCCCAACACCAATAACAGCTGCCCTGTATCTAGCTGCGGTGTTTCGTCCTTTCC
EA9	GCAGAGAGGGAGTGGCCAACTCCATCACTAG

EA10	GACCCCGTAATTGATTACTATTAATAACTAGACGCGAC TAGTAAAAAAAGTTGTGAATACCCTTCAAAG
EA11	TGTGCTCCTCGCGGATATACACTGTCCTG
EA12	TAGGCTGGAGGGCTATTTCAAGCAGACCAAC
EA13	TAATACGACTCACTATAGGGTCATCAGCAAAGAGCTC ATAAAGTTTCTTC
EA14	TCTCAATGGGTATTTGGACA

APPENDIX C

PLASMID MAPS OF CONSTRUCTS

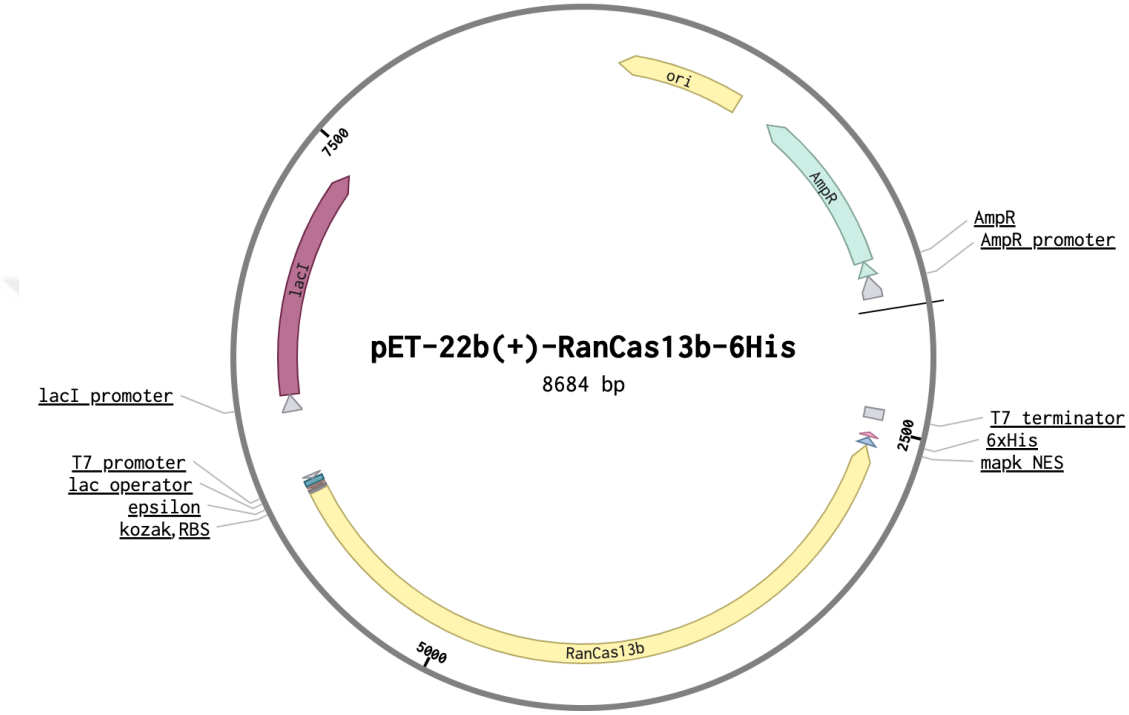

Figure C. 1: The schematic illustration of pET-22b(+)-RanCas13b-6His plasmid

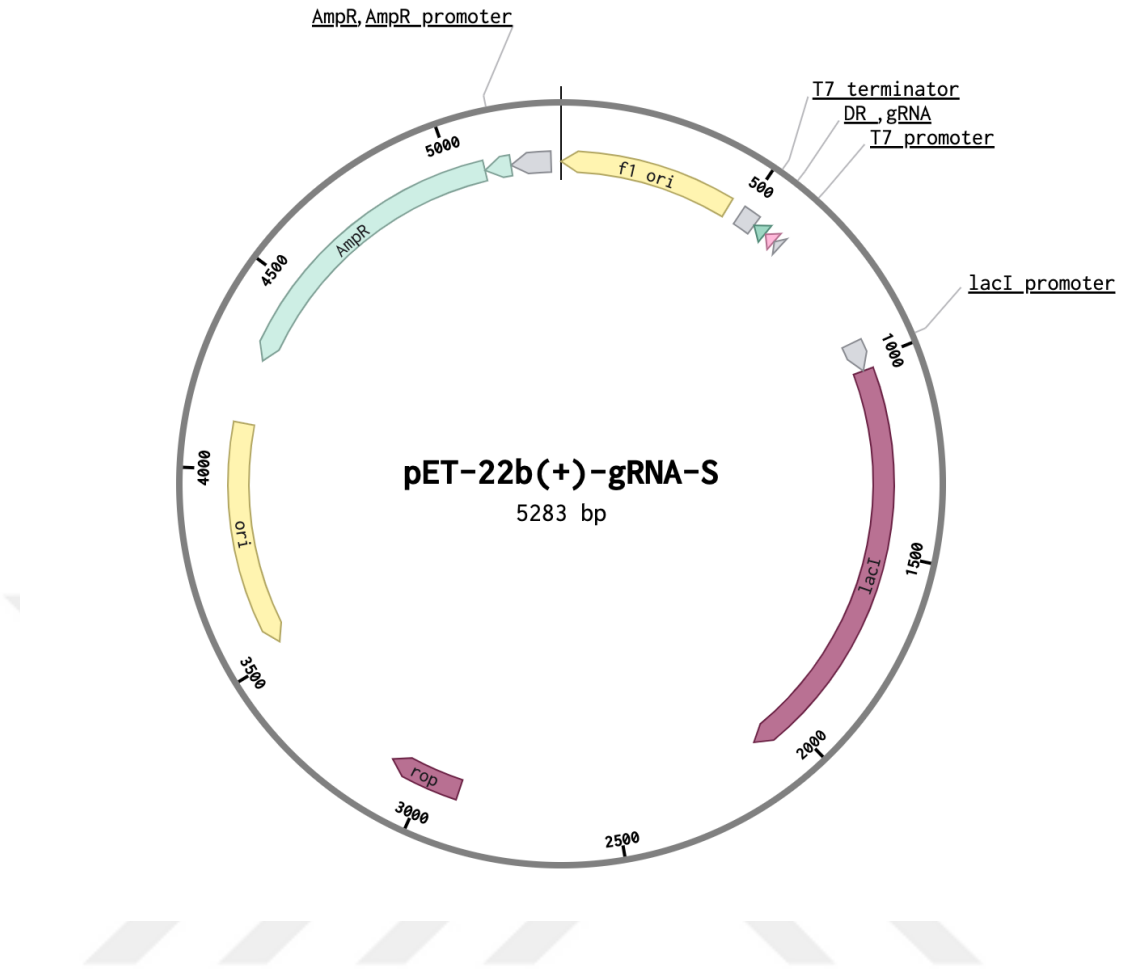

Figure C. 2: The schematic illustration of pET-22b(+)-S1gRNA plasmid

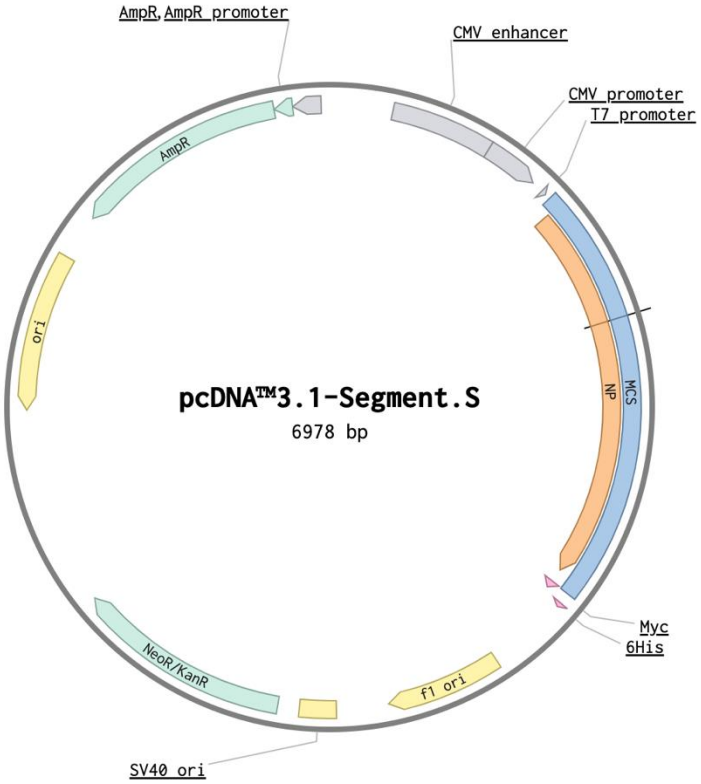

Figure C. 3: The schematic illustration of pcDNA™3.1-Segment.S plasmid

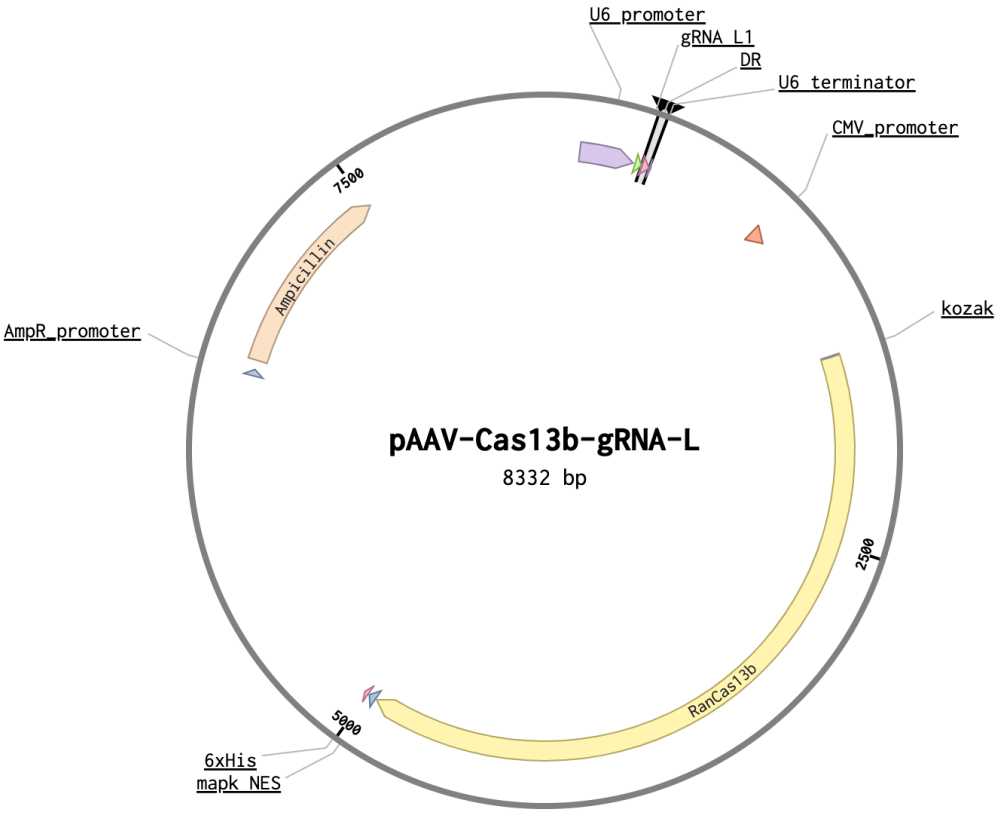

Figure C. 4: The schematic illustration of pAAV-Cas13b-gRNA-L plasmid

APPENDIX D

SEQUENCING RESULTS

Next-generation sequencing (NGS) was conducted for sequence analysis. To facilitate the identification of mismatched bases, the consensus sequence derived from NGS results was aligned using the Geneious Application and then uploaded to Benchling to compare the matching status of the plasmid sequence.

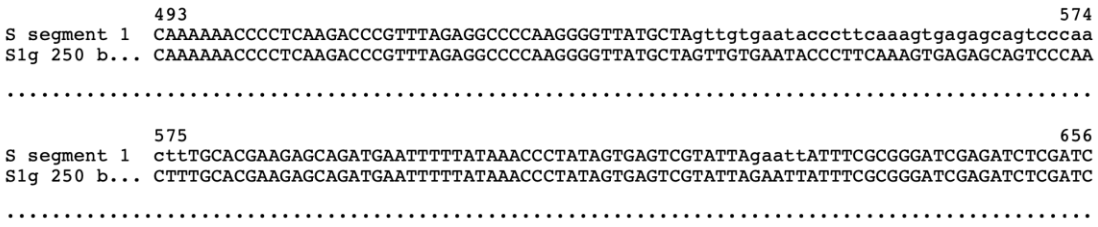

Figure D. 1: Sequencing result of pET-22b(+)-S1gRNA plasmid

```
            2707                                                                2788
pAAV-cas13b  agaatcgccaagtacccttataactccggcttcgtggcccacgcctttatctctgtgcacgagctgctgcctctgatgttct
pAAV-Cas1... AGAATCGCCAAGTACCCTTATAACTCCGGCTTCGTGGCCCACGCCTTTATCTCTGTGCACGAGCTGCTGCCTCTGATGTTCT

.....................................................................................

            2789                                                                2870
pAAV-cas13b  accagcacctgaccggcaagagcgaggacctgctgaaggagacagtgcggcacatccagagaatctataaggacttcgagga
pAAV-Cas1... ACCAGCACCTGACCGGCAAGAGCGAGGACCTGCTGAAGGAGACAGTGCGGCACATCCAGAGAATCTATAAGGACTTCGAGGA

.....................................................................................

            2871                                                                2952
pAAV-cas13b  ggagcggatcaataccatcgaggatctggagaaggcaaaccagggcagactgccactgggagcctttcccaagcagatgctg
pAAV-Cas1... GGAGCGGATCAATACCATCGAGGATCTGGAGAAGGCAAACCAGGGCAGACTGCCACTGGGAGCCTTTCCCAAGCAGATGCTG

.....................................................................................

            2953                                                                3034
pAAV-cas13b  ggcctgctgcagaataagcagcctgatctgtccgagaaggccaagatcaagatcgagaagctgatcgccgagacaaagctgc
pAAV-Cas1... GGCCTGCTGCAGAATAAGCAGCCTGATCTGTCCGAGAAGGCCAAGATCAAGATCGAGAAGCTGATCGCCGAGACAAAGCTGC

.....................................................................................

            3035                                                                3116
pAAV-cas13b  tgtctcacaggctgaacacaaagctgaagagctccccaaagctgggcaagcggagagagaagctgatcaagacaggcgtgct
pAAV-Cas1... TGTCTCACAGGCTGAACACAAAGCTGAAGAGCTCCCCAAAGCTGGGCAAGCGGAGAGAGAAGCTGATCAAGACAGGCGTGCT

.....................................................................................

            3117                                                                3198
pAAV-cas13b  ggccgactggctggtgaaggatttcatgcgctttcagcccgtggcctacgacgcccagaatcagcctatcaagtctagcaag
pAAV-Cas1... GGCCGACTGGCTGGTGAAGGATTTCATGCGCTTTCAGCCCGTGGCCTACGACGCCCAGAATCAGCCTATCAAGTCTAGCAAG

.....................................................................................

            3199                                                                3280
pAAV-cas13b  gccaactccaccgagttctggtttatcaggcgcgccctggccctgtacggaggagagaagaataggctggagggctatttca
pAAV-Cas1... GCCAACTCCACCGAGTTCTGGTTTATCAGGCGCGCCCTGGCCCTGTACGGAGGAGAGAAGAATAGGCTGGAGGGCTATTTCA

.....................................................................................

            3281                                                                3362
pAAV-cas13b  agcagaccaacctgatcggcaacacaaatccacacccttcctgaacaagtttaattggaaggcctgcaggaatctggtgga
pAAV-Cas1... AGCAGACCAACCTGATCGGCAACACAAATCCACACCCCTTCCTGAACAAGTTTAATTGGAAGGCCTGCAGGAATCTGGTGGA

.....................................................................................

            3363                                                                3444
pAAV-cas13b  tttctaccagcagtatctggagcagcgcgagaagtttctggaggccatcaagaaccagccatgggagccctaccagtattgc
pAAV-Cas1... TTTCTACCAGCAGTATCTGGAGCAGCGCGAGAAGTTTCTGGAGGCCATCAAGAACCAGCCATGGGAGCCCTACCAGTATTGC

.....................................................................................

            3445                                                                3526
pAAV-cas13b  ctgctgctgaagatccctaaggagaacaggaagaatctggtgaagggatgggagcagggaggaatctctctgccacggggcc
pAAV-Cas1... CTGCTGCTGAAGATCCCTAAGGAGAACAGGAAGAATCTGGTGAAGGGATGGGAGCAGGGAGGAATCTCTCTGCCACGGGGCC

.....................................................................................

            3527                                                                3608
pAAV-cas13b  tgtttaccgaggccatcagagagacactgtctgaggacctgatgctgagcaagccaatccgcaaggagatcaagaagcacgg
pAAV-Cas1... TGTTTACCGAGGCCATCAGAGAGACACTGTCTGAGGACCTGATGCTGAGCAAGCCAATCCGCAAGGAGATCAAGAAGCACGG

.....................................................................................
```

Figure D. 2: Sequencing result of pAAV-Cas13b plasmid, partial sequence of Cas13

```
            165                                                                 246
Mlu1Gibso... GGTTCCTGCGGCCGCaGGTACCgagggcctatttcccatgattccttcatatttgcatatacgatacaaggctgttagagag
L1gRNA.Sa... GGTTCCTGCGGCCGCAGGTACCGAGGGCCTATTTCCCATGATTCCTTCATATTTGCATATACGATACAAGGCTGTTAGAGAG

.....................................................................................

            247                                                                 328
Mlu1Gibso... ataattagaattaatttgactgtaaacacaaagatattagtacaaaatacgtgacgtagaaagtaataatttcttgggtagt
L1gRNA.Sa... ATAATTAGAATTAATTTGACTGTAAACACAAAGATATTAGTACAAAATACGTGACGTAGAAAGTAATAATTTCTTGGGTAGT

.....................................................................................

            329                                                                 410
Mlu1Gibso... ttgcagttttaaaattatgttttaaaatggactatcatatgcttaccgtaacttgaaagtatttcgatttcttggctttata
L1gRNA.Sa... TTGCAGTTTTAAAATTATGTTTTAAAATGGACTATCATATGCTTACCGTAACTTGAAAGTATTTCGATTTCTTGGCTTTATA
```

Figure D. 3: Sequencing result of pAAV-Cas13b-gRNA-L plasmid

APPENDIX E

ADDITIONAL REACTION RECIPES

Table E. 1: Lysogeny Broth (LB) Growth Medium and LB Agar Recipe

Component	**Amount**
Yeast Extract	5 g
Sodium Chloride (NaCl)	10 g
Tryptone	10 g
Agar (for LB agar)	15 g
Water	1000 ml

Table E. 2: PCR reaction mix recipe with Q5

Component	**Amount (for 25 µl)**
5X Q5 Reaction Buffer	5 µl
10 mM dNTP	0.5 µl
10 µM Forward Primer	1.25 µl
10 µM Reverse Primer	1.25 µl
Template DNA	0.5 ng – 0.5 µg
Q5 DNA Polymerase	0.5 µl
Nuclease Free Water	Up to 25 µl

Table E. 3 Double Digestion Reaction

Component	**Amount (for 50 µl)**
10x Cut Smart Buffer	5 µl
DNA	2.5 µg
Restriction Enzyme 1	1 µl
Restriction Enzyme 2	1 µl
Nuclease Free Water	Up to 50 µl

Table E. 4 Gibson Assembly Mixture (1.33X)

Component	**Amount**
Taq Ligase (40 U/µl)	50 µl
5X Isothermal Buffer	100 µl
T5 Exonuclease (1 U/µl)	2 µl
Phusion Polymerase (2 U/µl)	6.25 µl
Nuclease Free Water	216.75 µl

Table E. 5: TSS Buffer Recipe

Component	**Amount**
PEG 8000	5 g
1M $MgCl_2$	1.5 ml
2.5 ml DMSO	2.5 ml
LB Medium	Up to 50 ml

Table E. 6: 10X TBE Buffer Recipe

Component	**Amount**
Tris Base	121.1 g
Boric Acid	61.8 g
EDTA	7.1 g

Table E. 7: PCR Reaction Conditions of Q5 DNA Polymerase

Step	**Temperature**	**Duration**
Initial Denaturation	98 °C	30 seconds
Denaturation	98 °C	5 - 10 seconds
Annealing	50 - 72 °C	10 - 30 seconds
Extension	72 °C	30 seconds / kb
Final Extension	72 °C	2 minutes
Hold	4 °C	∞

Table E. 8: T4 Ligation Reaction

Component	**Amount**
10x T4 DNA Ligase Buffer	2 µl
Vector DNA	50 ng
Insert DNA	Equal molar to vector DNA (1:1)
T4 DNA Ligase	1 µl
Nuclease Free Water	Up to 20 µl

Table E. 9: *In vitro* Cleavage Assay Reaction Buffer A

Component	**Final Concentration**
HEPES	20 mM at pH = 7.0
KCl	50 mM
$MgCl_2$	2 mM
DTT	5 mM
Glycerol	5 %

Table E. 10: *In vitro* Cleavage Assay Reaction Buffer B

Component	**Final Concentration**
Tris - HCl	20 mM at pH = 7.5
NaCl	50 mM
$MgCl_2$	0.5 mM
DTT	5 mM
BSA	0.5 %

Table E. 11: *In vitro* Transcription (IVT) Reaction Recipe

Component	**Amount**	**Final Concentration**
10X Reaction Buffer	1.5 µl	0.75X
NTP	1.5 µl each	7.5 mM each
Template DNA	X µl	1 µg
T7 Polymerase Mix	2 µl	
DTT	1 µl	5 mM
Nuclease Free Water	Up to 20 µl	

Table E. 12: Cas13b Storage Buffer

Component	**Final Concentration**
Tris - HCl	50 mM at pH = 7.5
NaCl	600 mM
DTT	2 mM
Glycerol	10 %

Table E. 13: *In Vitro* Cleavage Reaction Mix

Component	**Amount**
Reaction Buffer (10X)	3 µl
gRNA	10 nM
Cas13b	10 nM
Target RNA	1 nM
RNase Inhibitor (40U)	0.8 µl
Nuclease Free Water	Up to 30 µl